CUMMULATIVE FINAL REPORT FOR

THE UNIVERSITY OF CENTRAL FLORIDA

COVERING THE PERIOD OF 15-JUN-2007 TO 15-SEP-2009

Materials for Eye and Sensor Protection

JOSEPH W. PERRY and SETH R. MARDER
School of Chemistry & Biochemistry
Georgia Institute of Technology
901 Atlantic Drive
Atlanta, GA 30332-0400

Phone: 404-385-6046 (JWP); 404-385-6048 (SRM)
Fax: 404-385-6057 (JWP); 404-894-5909 (SRM)
E-mail: joe.perry@chemistry.gatech.edu; seth.marder@chemistry.gatech.edu

PART A.

OBJECTIVE:

Utilize the excited-state absorption of phthalocyanine (Pc) compounds to create optical-power limiting films in the visible region (400-700nm).

APPROACH:

Develop a method to prevent aggregation of Pcs in concentrated solution and films. Identify polymer host for Pc films with good Pc compatibility, processibility and film-forming characteristics. Cast films with high Pc concentration, low Pc aggregation and high (60-70%) light transmission in the spectral region of interest. Demonstrate optical power limiting of nanosecond laser pulses in the visible region.

SUMMARY

A polymer host and solvent system was identified as suitable for film formation with high concentration of dendronized Pcs. A casting method was developed and films were made with high concentrations of various dendronized Pcs. Several films were of good optical quality and UV/vis spectra were taken of these films.

RESULTS

Phthalocyanines are of particular interest for visible region optical power limiting due to the fact that they have a weak S_0-S_1 transition over much of the visible spectrum while they possess strong S_1-S_n and T_1-T_n transitions in the same region. This property indicates that Pcs may be useful for optical limiting throught reverse saturable absorption. However, they tend to aggregate at high concentration, which results in loss of the useful absorption properties. The Pcs shown in Figure A below have dendrimer appendages attached to prevent aggregation of Pcs at high concentration in solution and films.

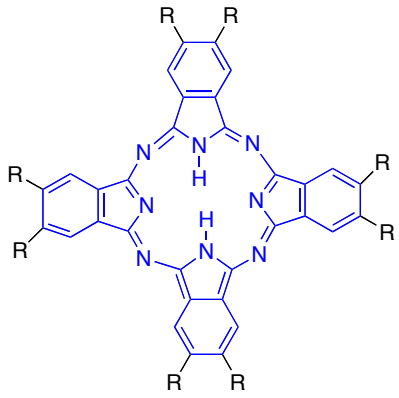

(a)

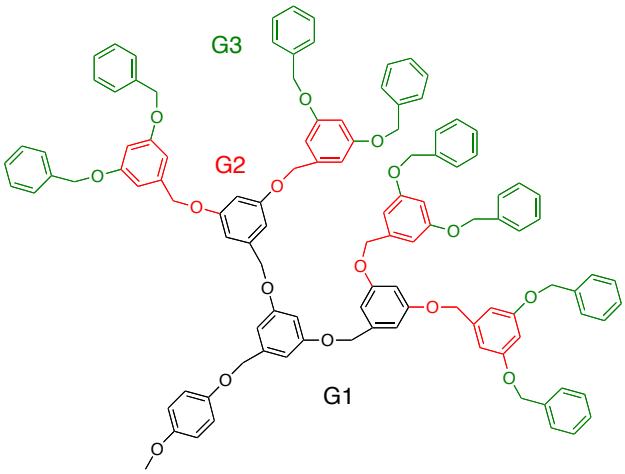

(b)

Figure A: **(a)** Phthalocyanine and **(b)** dendrimer substituent. In the names used for the various dendronized Pcs, G1Pc has only the black portion of the dendrimer attached to each R site on the Pc; G2Pc has both the black and the red portion, and G3Pc has the black, red and green portions.

In Figure B the effectiveness of the dendrimer groups can be observed: the G3Pc (G3 in the plot) shows the most detail in its spectrum and the fewest sings of aggregation (broadening and blue shifting of the red peak). A film of any of the dendronized Pcs with spectral features similar to that of the G3Pc in Figure B is the desired product.

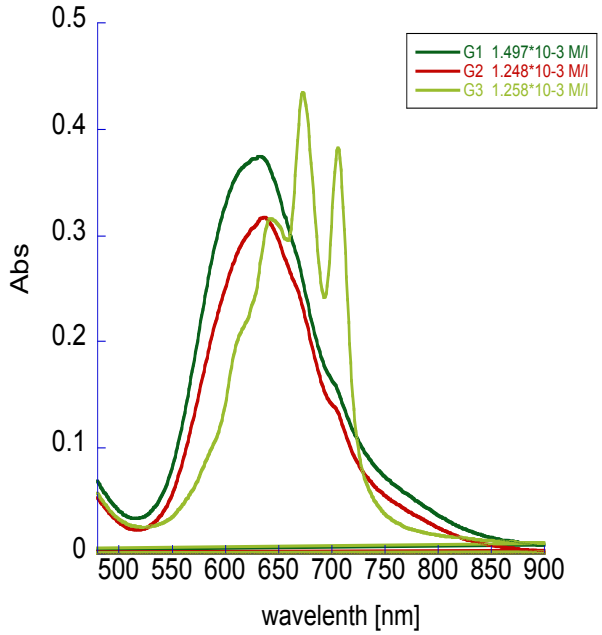

Figure B: UV/vis absorption of dendronized phthalocyanine free bases in toluene, at similar concedntrations. The G3Pc is the only one not to show significant signs of aggregation.

Two methods of film casting were used in this study: spin-casting and drop casting. In the former, the polymer/solvent/chromophore solution was deposited onto a clean glass slide, which was spun on an orthogonal axis to remove excess and to flatten and dry the film. In the latter, the polymer/solvent/chromophore solution was dropped by a pipette onto a clean glass slide and allowed to dry very slowly in a solvent saturated atmosphere. Photographs of films made by these methods are shown in Figure C. As can be seen in Figure C and in the film spectra in Figure D, spin-casting produced films that were of good optical quality, but were very thin and therefore had a visible transmittance too high to be useful for optical limiting. Drop-casting was therefore chosen as the film casting method. After a number of other trials, the solvent/polymer system was chosen to be cyclopentanone with amorphous polycarbonate.

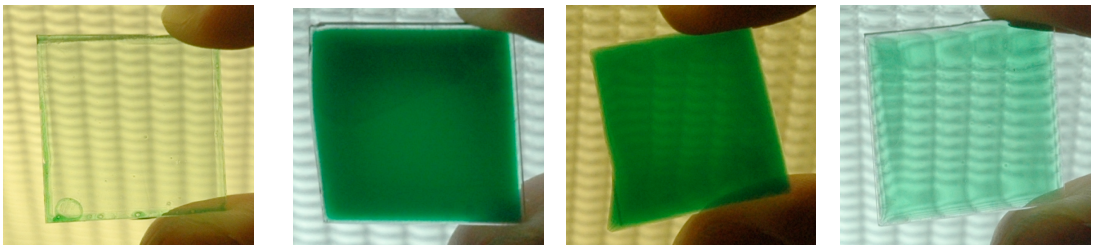

Figure C: Pictures of several of the films made. **(a)** Spin-cast G3Pc - 9.83% by weight. **(b)** Drop-cast G3Pc – 9.72% by weight. **(c)** Drop-cast G3Pc – 5.13% by weight. **(d)** Drop-cast G3Pc – 1.36% by weight. Note the opacity of (b) and (c) caused by phase-separation of the polymer and phthalocyanine.

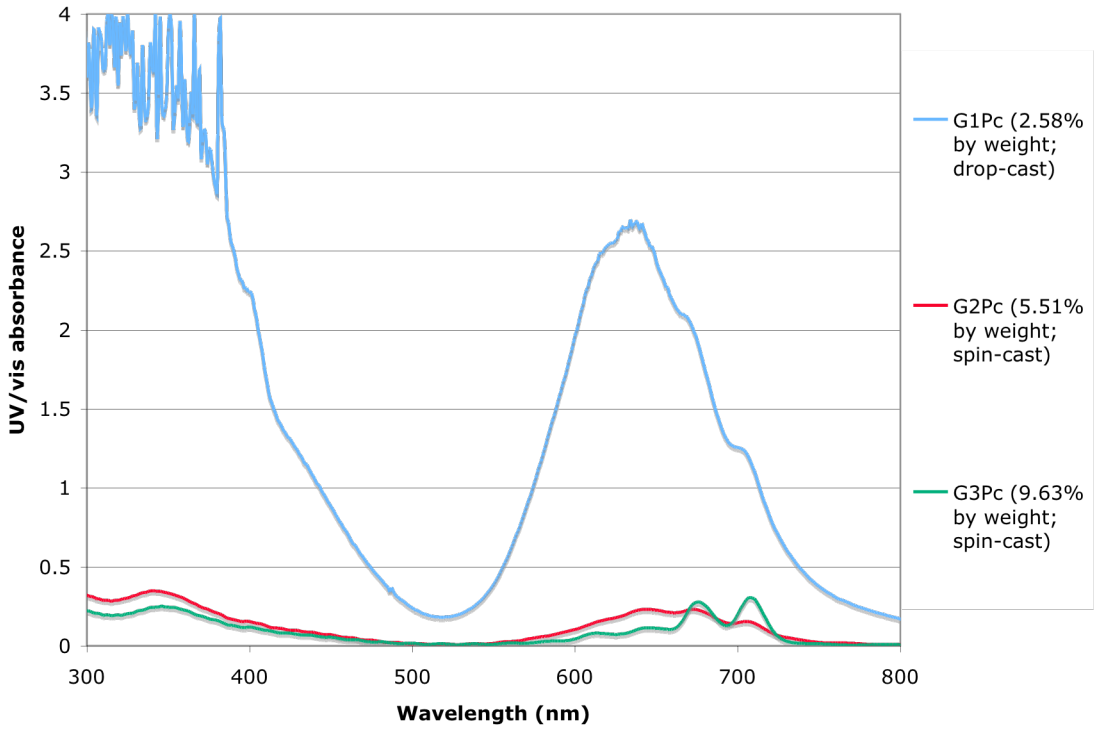

Figure D: UV/vis plots of representative films of the three dendronized phthalocyanines. Note that the molar concentration of the phthalocyanines is roughly equivalent in all three films. The drop-cast film shows much more absorption due to its being much thicker. The only film not to show signs of aggregation is G3Pc.

Several films with differing concentrations of G3Pc were made by drop-casting in order to get an optical quality film with non-aggregated G3Pc and a T_{532} (light transmission at 532nm) of 60-70% (UV/vis abs = 0.22-0.155). Pictures of these films are in (b), (c), and (d) of Figure C. As can be seen in the figure, (b) and (c) are relatively opaque, due to phase separation of the components of the film, while (d) is of good optical quality. The former two also possess low T_{532}, as shown in Figure E. Figure E contains UV/vis absorbance and transmittance spectra of three G3Pc films.

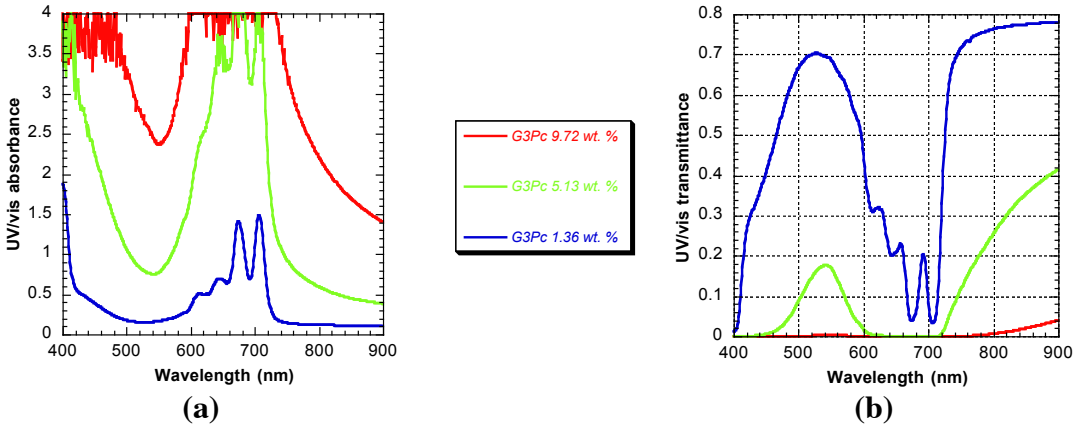

Figure E: (a) Absorbance and (b) transmittance plots of the drop-cast G3Pc films in Figure C. Aggregation is not observed in the absorbance, while for the lowest weight-percent G3Pc film, T_{532}=70%.

CONCLUSIONS

The dendronized Pc G3Pc has been shown to form good optical quality films in an amorphous polycarbonate host polymer. A method has been developed to make films of consistently good quality with high transmittance at 532nm. Further wok to be done includes optical-power limiting studies with nanosecond laser pulses at 532nm.

PART B

OBJECTIVE:

Understand how to improve the performance of opto-electronic materials by using polymers with well-defined structures.

APPROACH:

Investigate multichromophoric systems for photoinduced charge generation or energy transfer and optical absorption. Perform spectroscopic characterization of charge generation, transient optical properties, and optical limiting properties.

MILESTONES:

To develop materials for efficient charge carrier generation or energy transfer and long lifetimes. To develop high sensitivity, broadband, high dynamic range nonlinear absorptive materials for optical limiting.

ACCOMPLISHMENTS

Performed optical power limiting and transient absorption spectroscopy on a dendron substituted Ru phthalocyanine that showed strong optical power limiting at 500 nm in solution.

RESULTS

We have performed transient and nonlinear optical studies of a dendron substituted Ru phthalocyanine ($RuG3_2Pc$), whose structure is shown in Fig. 1, that was synthesized by the Marder group. The linear electronic absorption spectrum of $RuG3_2Pc$ in toluene is shown in Figure 2. The spectrum shows a Q-band absorption at 635 nm and a minimum at 486 nm. The Q-band is significantly blue shifted and broader compared to typical main group ions such as Si, Sn, or In or transition metals such as Zn. Optical power limiting data were taken on $RuG3_2Pc$ in toluene using an f/5 optical geometry, 475 and 500 nm, 5 ns laser pulses, and a 10 Hz repetition rate, as shown in Fig. 3. Significant optical limiting was observed at both wavelengths. The initial transmission at 475 nm

was 70% and at 500 nm was 46%. The suppressions (T_{linear}/T_{Emax}) were 5.8 and 42 at 475 and 500 nm, respectively. The responses for $RuG3_2Pc$ are compared with that of an $InClPc(t\text{-}butyl)_4$ solution in toluene with a 70% transmission at 532 nm where the limting data were taken; $InClPc(t\text{-}butyl)_4$ is known to be a high performance optical limiting dye

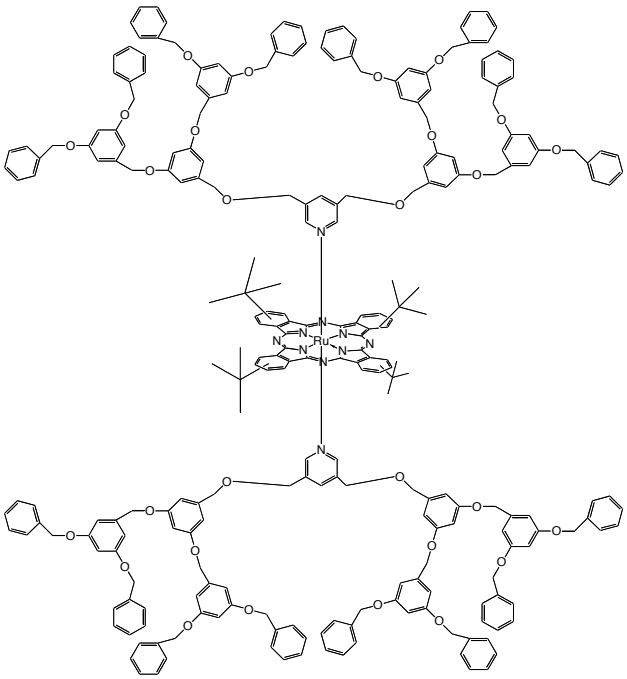

Figure 1. Structure of a dendrimer substituted Ru phthalocyanine ($RuG3_2Pc$).

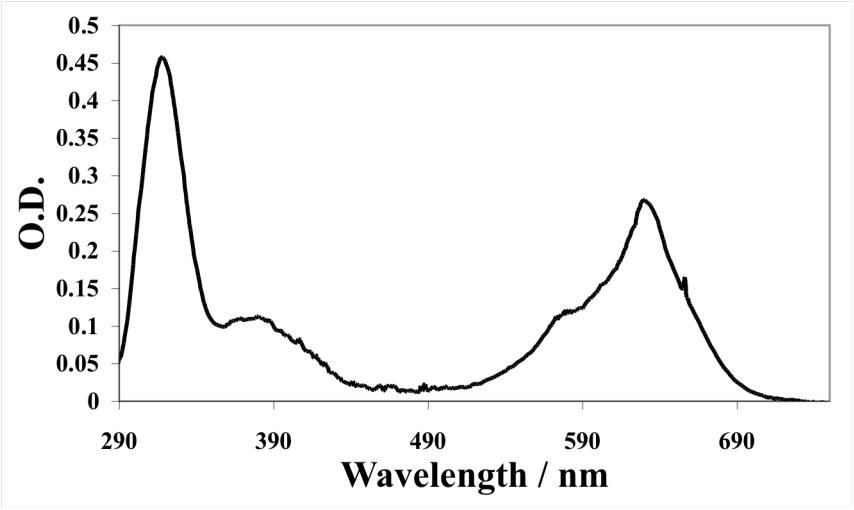

Figure 2. Visible absorption spectrum of dendrimer substituted $RuG3_2Pc$ in toluene solution, as used for transient absorption spectroscopy, see below.

at this wavelength. The suppression of the InClPc(t-butyl)$_4$ solution was observed to 15 at 532 nm in the same geometry.

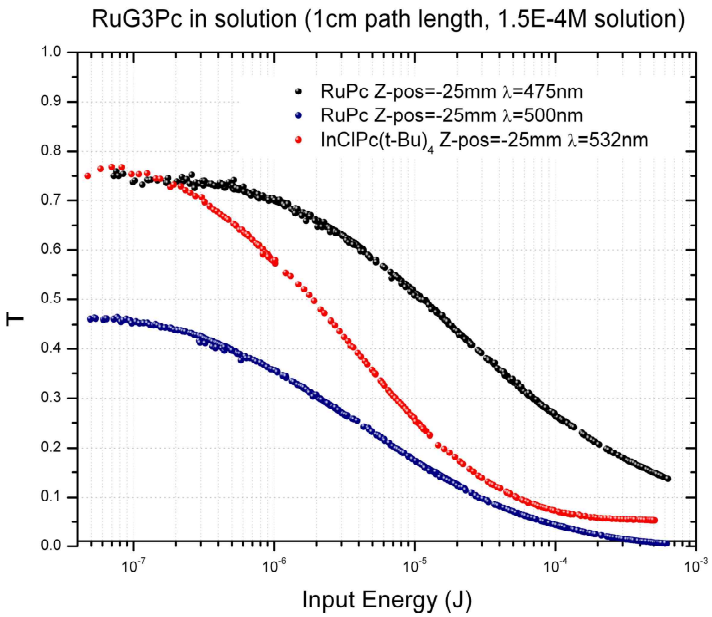

Figure 3. Optical power limiting data for the dendrimer substituted RuG3$_2$Pc in toluene solution at 475 and 500 nm, and a comparison with InClPc(t-butyl)$_4$ at 532 nm, for 5 ns laser pulses.

CONCLUSIONS

We have shown that RuG3$_2$Pc shows strong optical limiting at ~500 nm for nanosecond laser pulses consistent with a reverse saturable absorption mechanism. It is likely that charge transfer interactions between the Ru^{2+} central metal ion and the Pc ligand play a role in the spectroscopy of this system. Transient absorption data provide some initial support for a RSA mechanism with an excited state that decays on the nanosecond timescale.

.

PART C.

One- and Two-Photon Properties of Donor/Acceptor Substituted Distyryl,diphenylethynylbenzene Cruciforms

ABSTRACT Cross-shaped 1,4-distyryl-2,5-diphenylethynylbenzenes (cruciforms) with di-n-butylamino donors on the styryl arms, or on all arms, and varying electron acceptor substitutions on the phenylethynyl arms, as well as with no electroactive substituents have been synthesized and investigated using one-photon and two-photon fluorescence excitation spectroscopy. The cruciform without donor or acceptor substitution shows distinct one-photon pp* absorption bands for the different arms The attachment of electron-donating groups to the styryl arms and electron-withdrawing groups to the phenylethynyl arms results in the lowest-energy 1PA band taking on significant charge-transfer character. As the acceptor strength in donor/acceptor structure is increased from weak to moderate, δ_{max} increases while $\lambda_{max}^{(2)}$ shows a bathochromic shift, and a relatively weak, long-wavelength 2PA peak rises at longer wavelengths relative to the $\lambda_{max}^{(2)}$. In a donor/acceptor cruciform with a strong acceptor, the $\lambda_{max}^{(2)}$ shows a hypsochromic shift, while the long-wavelength peak rises relative to δ_{max}. The trends observed in the spectra result from the changing nature of the interarm coupling in the chromophore: as the donor/acceptor pattern is introduced and acceptor strength is increased, the cruciform S_1 excited state changes from weakly mixed, localized MOs to strongly coupled degenerate charge transfer (CT) states. With only donor or no substituent groups, the MOs of the arms are weakly mixed. With donor and strong acceptor groups, the MOs of the arms are strongly mixed by coupled degenerate CT

states. With donor and weak or moderate acceptor groups, the arms undergo a combination of the two types of mixing.

The tetra-donor substituted cruciform leads to two bands in the two-photon absorption (2PA) spectrum associated primarily with 2PA transitions in the phenylethynyl and styryl arms, and a hypsochromic shift of the peak 2PA wavelength ($\lambda_{max}^{(2)}$), but no increase in the peak cross-section (δ_{max}) compared to a linear D-π-D chromophore. Studies of a series of cruciforms and a set of linear conjugated model compounds indicate that non-degenerate conjugation in the arms of the chromophore leads to significant differences in optical properties compared to those with degenerately conjugated arms. The one-photon absorption (1PA) spectra of the cruciforms are broader and yet more featured than those of compounds with degenerate conjugation. These observations suggest that the introduction of non-degenerate conjugation results in weak to moderate mixing of the π and π* excited states of the linear components of cruciform chromophores for cruciforms with no donor/acceptor substituents or four identical donor substituents.

Introduction

Understanding relationships between molecular structure and two-photon absorption (2PA) properties is of fundamental chemical interest.[1-5] Such understanding also has significance for the use of molecular materials in applications such as fluorescence imaging[6-8] and lithographic micro- and nano-fabrication with three-dimensional spatial resolution,[9-13] as well as dynamic range compression in optical signal processing[14] and optical power limiting.[15-17] Substantial progress has been made in elucidating structure-

property relationships for two-photon absorption, especially for dipolar[2] and quasi-linear quadrupolar conjugated molecules[1,17-21] such as compounds **1a** and **1b** in Figure 1. For quasi-linear quadrupolar molecules, experimental and theoretical studies have demonstrated correlations between the peak two-photon absorption cross section (δ_{max}) for the lowest energy two-photon state, and the degree of intramolecular charge transfer upon excitation between the ground state and the low lying excited state,[1] as well as the conjugation length of the chromophore.[19] For quadrupolar chromophores, a three-level approximation for the peak, on-resonance 2PA cross section for the 2PA transition to excited state e′ results in the following proportionality relationship:[1,19,22]

$$\delta_{g\rightarrow e'} \propto \frac{M_{ge}^2 M_{ee'}^2}{(E_{ge} - \hbar\omega)^2 \Gamma_{ge'}} \qquad (1)$$

In Equation 1, M represents a transition dipole moment between two electronic states, E represents the difference in energy between states indicated by the subscripts, $\hbar\omega$ is the excitation photon energy, $\Gamma_{ge'}$ is a damping term, and the subscripts g, i and e' refer to the ground electronic state, the lowest symmetry-allowed one-photon state and the lowest two-photon allowed state, respectively. This approximate relationship provides insight into the major factors governing the peak cross section of the lowest energy 2PA band in quadrupolar compounds. The qualitative trends that have emerged from experimental and computational studies are that δ_{max} increases with: 1) increased conjugation length due to increases in M_{ge} and decreases in the detuning term ($E_{ge} - \hbar\omega$), and 2) increased degrees of symmetric intramolecular charge transfer that give rise to increases in $M_{ee'}$.

Recently, 2PA structure-property relationships have been investigated for organic chromophores with conjugation extending in two or three dimensions (2D or 3D). It has been reported that branched structures and other types of superstructures (in which the individual units are themselves 2PA chromophores) may display cooperative enhancement of 2PA due to electronic interactions between the individual units. Some fully conjugated superstructure systems for which cooperative enhancement of 2PA has been reported include porphyrin dimers linked through conjugated bridges,[23-26] porphyrins linked in a macromolecular ring motif[27,28] and porphyrin ladder polymers.[29,30] These structures have been reported to show increases ranging between a factor of 3 to a factor of ~60 in δ_{max}/chromophore unit with respect to the δ_{max} of the individual chromophores they are made from. This phenomenon that has been ascribed to resonant interactions between the units and to increases in the transition dipole moments between the states participating in the 2PA transition. In the case of branched chromophore structures such as octupolar[31-38] or dendritic[39-42] structures, the question of enhancement is more complex. In general, for these structures, the effects of the branched structure on the 2PA properties of each individual unit is strongly dependent on the nature and extent of the inter-unit electronic coupling.[43] Various types of coupling through conjugated linkers or through shared groups have been reported to have negligible impact[44] or approximately 2- to 4-fold enhancement[34,40,45,46] or a slight reduction[33,47] of δ_{max}/chromophore unit, as well as broadening[46,48,49] and shifts[46,48] of the 2PA spectrum.

Cruciform chromophores such as compounds **3**-**6** in Figure 1 are another prototypical form of two-dimensional conjugated structure, which may be thought of as two linear chromophores coupled directly through a central ring. Two-photon absorption spectra

have been reported for systems with arms extended via four double-bonded[50,51] or four triple-bonded[52,53] linkages. These recent studies have shown δ_{max} values of 1100 GM at 700 nm for an all-double bonded cruciform with four dialkylamine donor groups (compound **3**)[50,51] and 570 GM at approximately 700 nm for an all-triple bonded cruciform with four dialkylamine substituents (compound **5**).[52,53] In the case of **3**, it was found that there is no enhancement of the δ_{max}/chromophore unit or the integrated 2PA band per chromophore unit as compared with the corresponding linear compound **1a**, although the 2PA band does show a slight blue shift and broadening.[50,51] Rumi *et al*.[50,51] applied Kasha's molecular exciton model to understand the one- and two-photon properties of cruciform compounds with four identical double-bonded arms such as **3**, treating the system as a pair of coupled linear quadrupolar chromophores such as **1a**. This model predicted that δ_{max} for the case of a cruciform compound with degenerate arms is dependent on the angle between the arms, and the strength and sign of the coupling interaction. Based on the estimate of the coupling obtained from the 1PA spectrum of **3**, the value of δ_{max} would actually be smaller than the sum of the δ_{max} of the corresponding linear chromophores, corresponding to the observed spectra. This indicates that the cruciform architecture alone is not sufficient to lead to an increase in δ_{max} for the low energy two-photon states.

In this paper, we report on a detailed study of a series of cruciforms based on 1,4-distyryl-2,5-bis(phenylethynyl)benzene possessing non-degenerate conjugated arms (compound **13**) as well as four symmetrically substituted donor groups (compound **14**) or varying donor/acceptor (D/A) substitution (compounds **15**-**20**). Such D/A substituted cruciforms, with conjugation via double bonds in one arm and triple bonds in the other,

have been shown to exhibit interesting charge-transfer based metal-ion responsive optical properties.[54-58] Based on literature values for the Hammett parameters[59,60] of the substituents, the acceptor groups used in **16**-**20** increase in electron-accepting strength in the following pattern: *o*-CF_3 ≈ *p*-CF_3 < di-*m*-CF_3 ≈ *p*-CN < *p*-NO_2. There are several basic questions of interest regarding the optical properties of these cruciform systems including: 1) the role of electronic coupling for the case of two energetically non-degenerate chromophoric units; 2) the effect of the degree of charge transfer associated with variation of the strength of the electron accepting groups; and 3) the impact of coupling of pairs of charge-transfer pathways within the cruciforms, which we have addressed through a combination of one- and two-photon spectroscopic studies on a systematically varied set of cruciforms and double- or triple-bond containing linear model compounds.

Experimental

Synthesis: The synthesis and characterization of compounds **11**, **12**, **14**, and **20** are detailed in the Supporting Information. The synthesis of compounds **13** and **15-19** as well as the necessary starting materials have been previously reported.[54,55,61,62]

One-photon spectroscopy: All cruciform and linear model compound samples were studied in toluene (Sigma-Aldrich, spectroscopic grade) solutions. Solutions of fluorescence quantum yield standard compounds were made using Sigma-Aldrich spectroscopic grade solvents, except as noted. One-photon absorption spectra were obtained with a diode array spectrometer (Hewlett-Packard 8453) and fluorescence emission spectra were measured using a spectrofluorimeter (Spex Fluorolog II). Values of the peak molar extinction coefficient, ε_{max}, were determined from Beer's law plots over

the concentration range of 1 x 10^{-7} M to 5 x 10^{-4} M. The fluorescence quantum yields, η_{fl}, were obtained with solution concentrations of approximately 10^{-7} M. The fluorescence quantum yields reported are averaged results obtained from at least two independently prepared solutions using 1,4-bis(2-methylstyryl)-benzene (Sigma-Aldrich, 99%) in cyclohexane{Berlman} (compounds **11**-**13**) and 9,10-bis(phenylethynyl)-anthracene (Sigma-Aldrich, 97%) in cyclohexane[63] (compounds **14**-**20**) as standards.

Two-photon spectroscopy: The optical setup used for nanosecond two-photon fluorescence excitation spectroscopy has been described previously.[19] Two-photon fluorescence excitation spectra were obtained using a reference based method.[64] An optical parametric oscillator (Spectra-Physics, MOPO 730) that was pumped by a nanosecond Q-switched Nd:YAG laser (Spectra-Physics, Quanta-Ray Pro-250) running at 10 Hz was used as the excitation source. Solution concentrations were in the range of 50-100 μM. The two-photon excitation spectra reported in this paper are the average of at least three independent acquisitions of 200 pulses each at each wavelength reported. The dependence of the 2PEF signal on excitation power was tested for each compound and found to be quadratic over the range of excitation intensities used (0.05 - 0.15 mJ/pulse). The reference compounds used were 1,4-bis(2-methylstyryl)benzene[65,66] in cyclohexane for the spectral region between 550-690 nm and fluorescein[64] (Acros, laser grade) in pH 11 NaOH (in deionized H_2O) for the spectral region between 685-1040 nm. The 2PA spectrum and cross section values of bis(2-methylstyryl)benzene reported in by Kennedy and Lytle[65] were reduced in scale by a factor of 10 as described by Fisher et al.[66]

Results

Synthesis and Characterization: A modular protocol was employed to synthesize cruciforms **13-20** (Scheme 1); this approach permits the introduction of a diversity of groups on the periphery of the cruciform core. Starting from the diiodo-bisphosphonate **7**, a Horner olefination with an aromatic aldehyde was used to form the distyryl branch of the cruciform. A subsequent Pd-catalyzed Sonogashira coupling of a diiodide (**9a-b)** with an aryl alkyne (**10a-g**) completed the formation of the conjugated core, furnishing cruciforms **13-20**. Complete synthetic details are provided in the Supporting Information.

One-photon Spectroscopy: The absorption spectra of compounds **11**-**14** are shown in Figure 3a. The spectra of compounds **11** and **12**, which serve as double bond and triple bond containing linear model compounds, show an absorption maximum at 329 nm for **11**, which is at somewhat higher energy than that of **12** (363 nm), as expected for a bis(phenylethynyl)-benzene chromophore as compared to a bis(styryl)-benzene chromophore. While the spectra of **11** and **12** each show only one prominent electronic absorption band in the wavelength range examined, both spectra exhibit vibronic structure, with a major vibrational frequency of about 1500 cm^{-1}. In contrast, the spectrum of the cruciform **13**, bearing no significant electron donor or acceptor groups, shows two distinct electronic absorption bands, with maxima at 332 nm and 376 nm, the latter of which has a smaller ε_{max} than the former, and also shows a low-energy shoulder similar to that observed in **12**. The symmetrically tetra-donor-substituted cruciform **14** also shows two distinct absorption bands**,** the higher (386 nm) and lower (430 nm) energy bands being bathochromically shifted by 4200 cm^{-1} and 2700 cm^{-1}, respectively, relative to those of **13**. This shift is a result of a reduction in the HOMO-LUMO gap caused by

destabilization of the HOMO by the alkylamine groups. The fluorescence emission spectra (see Figure 4) of all four of these compounds are very structured, with four vibronic transitions easily identifiable in each spectrum. A summary of the one-photon spectroscopic parameters of compounds **11**-**20** is presented in Table 1.

Donor/acceptor substitution of the nondegenerate cruciform backbone (**15**–**20)** results in significant changes in the 1PA spectra of the cruciforms (spectra of **15**, **16**, **19**, and **20** are shown in Figure 3b, see Supporting Information for spectra of **17** and **18**). The addition of the two donor groups along the distyryl arm in **15** results in an absorption spectrum wherein the lowest energy feature is bathochromically shifted by about 3200 cm^{-1} compared to that of the non-D/A substituted analogue **13**, whereas the higher energy band of **15** is only slightly red-shifted by approximately 450 cm^{-1} relative to the overall peak of **13**. In the D/A substituted compounds **16**-**20**, in which the acceptor strength is increased, several changes occur: 1) the peak position of the lower energy 1PA band remains roughly constant (within 10 nm), 2) the band shape of the lower energy band broadens with an increasing splitting of the lower energy shoulder relative to **15**, and 3) the higher energy band (at approximately 340-350 nm) red-shifts increasingly as the strength of the electron-acceptor group increases from m-CF_3, to cyano, to nitro. The fluorescence spectra (Figure 4) of the cruciforms show a systematic red shift upon donor or D/A substitution (**14** – **20**) as compared to **13**, and **16**-**20** show significantly greater Stokes shifts and less vibronic structure than **13**-**15**, as expected for transitions with significant intramolecular charge transfer character. The fluorescence quantum yields of the D/A substituted cruciforms are all approximately 0.7 with the exception of the nitro-substituted cruciform **20**, which has a much lower quantum yield of 0.005.

Two-photon Spectroscopy: The 2PA spectra were determined by the two-photon fluorescence excitation (2PFE) method. The 2PA data are summarized in Table 1. Figure 5a shows the spectra of the linear model compounds **11** and **12** with respect to that of **13** (cruciform core with only *p*-isopropyl substituents on the styryl arms). The δ_{max} of **12** was measured as 110 GM at the 2PA peak wavelength ($\lambda_{max}^{(2)}$) of 580 nm. In the case of **11** and **13**, the position of the 2PA peak is at or below the shortest excitation wavelength accessed in this study, 550 nm. The largest values of δ in the range measured were 160 GM for **11** and 150 GM for **13** at 550 nm. The 2PA spectrum of **13** is not consistent with a bathochromic shift relative to the 2PA spectrum of **12**, although the longer wavelength sides of both spectra are qualitatively similar. This will be addressed further in the discussion.

The addition of D/A groups to the arms of the cruciforms had significant effects on the 2PA spectra (Figure 5b). The spectrum of symmetrically tetra-donor substituted **14** has a δ_{max} of 1200 GM at a $\lambda_{max}^{(2)}$ of 700 nm, constituting an approximately 6-fold increase in δ_{max} and an approximately 3900 cm^{-1} bathochromic shift of $\lambda_{max}^{(2)}$ relative to that of **13**. The $\lambda_{max}^{(2)}$ is blue-shifted by 590 cm^{-1} and δ_{max} is similar, when compared to those reported[19,20,50,51] for the bis-donor linear compound **1a**. There is also a shoulder on the 2PA spectrum of **14** at 750 nm with a δ of 550 GM. In **15**, without donor groups on the triple-bonded arm of the cruciform core, the $\lambda_{max}^{(2)}$ shifts further to 770 nm, while the δ_{max} is reduced to 740 GM, still an approximately four-fold increase relative to the non-D/A substituted cruciform **13**. This $\lambda_{max}^{(2)}$ is red-shifted by 710 cm^{-1} and δ_{max} is reduced in magnitude compared to that of compound **1a**. Interestingly, while the $\lambda_{max}^{(2)}$ of **15** is red-

shifted by 1300 cm^{-1} from the peak of tetra-donor substituted **14**, it is rather close to the shoulder of **14** at 750 nm.

In **16** and **17**, the addition of inductive electron withdrawing CF_3 groups in the ortho or para positions on the terminal phenyls of the triple-bonded arm causes the phenyls to become electron deficient and act as weak electron acceptors. The $\lambda_{max}^{(2)}$ wavelengths display a red-shift with respect to **15** to about 810 nm, while the δ_{max} values are 640 GM and 730 GM, not significant changes given the experimental uncertainty in the measurement. When two CF_3 groups (in **18**) or one π-acceptor CN group (in **19**) are substituted on the same phenyl rings, the effective acceptor strength is increased. There is again a red shift of $\lambda_{max}^{(2)}$ (to 830 nm) but also an increase in δ_{max}, to 910 GM and 950 GM, respectively, and the 2PA band becomes somewhat narrower. However, upon addition of strong NO_2 electron acceptors in **20**, the $\lambda_{max}^{(2)}$ shifts to 770 nm and the δ_{max} is reduced. The 2PA spectrum of **20** is rather broad with weaker bands at ~880 and 970 nm. In the whole series of D/A cruciforms, there is a weak 2PA band that shifts from about 930 to 970 nm and increases in strength as the effective acceptor strength increases. There also appears to be a weak band at 880 nm in the spectrum of **20**.

Discussion

The 1PA spectra of the cruciforms examined in this paper show shifts in band positions and splittings of bands that reflect the nature and extent of electronic interactions between the different arms of the cruciforms. There is an increase in the separation of the bands that are correlated with the lowest energy $\pi \rightarrow \pi^*$ transitions of the vinyl and ethynyl arms in the unsubstituted cruciform, **13**, relative to those of the

corresponding linear model compounds, which we ascribe to an electronic coupling and mixing of the ππ* excited states of the different arms. There is also a red-shift of the average position of the bands, which is due to an overall stabilization of the excited states upon coupling of the two arms. A similar trend is observed for the fully terminal donor substituted cruciform, **14**, although in this case the center of the band positions is significantly red-shifted compared to **13**, due to the donor substitution. These results are again consistent with a mixing of the π* excited states of the different arms. The structure in the lower energy band of **13** and **14** is attributed to a vibronic progression.

Cruciforms **15**-**19** have terminal donor substituted vinyl arms and different terminal acceptors on the ethynyl arms. In addition to the increase in the separation of the high and low energy bands of these compounds, there is a splitting of the low energy band that is too large to be assigned to a vibrational mode energy. For these compounds there is likely a significant charge transfer (CT) contribution to the low energy band and we believe that the splitting is associated with a coupling of discrete charge transfer excitations. The low energy band in **15**-**19** broadens as the strength of the acceptor group goes from weak (**15**) to moderate (**19**), while the peak position stays relatively constant, leading to significant bathochromic shifts of the lowest energy features of the spectra. The higher-energy band of the cruciforms is at a similar position to the analogous acceptor substituted triple-bonded linear compound, where comparative data is available.{nguyen 1994} To obtain insight into these observations, we have modeled the spectra of the cruciforms using a molecular exciton approach for the π* excited states of the two arms and for the CT excited states that involve transfer of electron density from the donors to the acceptors on the different arms. The 1PA spectra were decomposed into

sets of π→π* and CT bands and the electronic transition energies were obtained by applying a Franck-Condon bandshape analysis. These results, together with the transition energies for the corresponding linear model compounds, were used to estimate the coupling energies and wavefunction mixing coefficients for the cruciforms.

Simple exciton analysis of cruciform electronic epectra. In the molecular exciton model, when two chromophores are in close proximity or are attached to each other, their electronic interaction leads to a mixing of the excited state wavefunctions and shifts or splittings of the electronic absorption bands of the combined chromophore.{kasha 1965; ferguson 1986} We have divided the cruciforms into two nondegenerate linear components associated with the ethynyl and vinyl arms linked in *para*- fashion on the central phenyl ring, similarly to what has been used previously for compounds **3** and **4**.{rumi jpcc 2008} This is somewhat approximate in that each arm shares the central phenyl ring. Figure 6 diagrams the interactions of the energetically non-degenerate π* excited states of chromophores **11a** and **12a**, which model **11** and **12**. Since the π→π* transition dipoles of the components are at an angle to each other, they satisfy the conditions of an oblique exciton{kasha 1965} and the component excited states mix to produce two 1PA-allowed excited states in **13a**.

As described in detail in the Supporting Information, the energies of the exciton excited states resulting from the interaction of non-identical components 1 and 2 is

$$E_{\pm} = \frac{E_e^{(1)'} + E_e^{(2)'}}{2} \pm \frac{\sqrt{(E_{eg}^{(1)} - E_{eg}^{(2)} + \Delta V^{diag})^2 + 4V^2}}{2} \qquad (2)$$

where E_+ and E_- are the exciton states formed by symmetrical and antisymmetrical combinations of the excited states of the components, $E_e^{(1)'}$ and $E_e^{(2)'}$ are defined as the

excited state energies of the individual units including diagonal energy shifts due to Van der Waals interaction of the two units, $E_{eg}^{(1)}$ and $E_{eg}^{(2)}$ are the $g \rightarrow e$ transition energies of components 1 and 2, and $\Delta V^{diag} = V_{eg}^{diag} - V_{ge}^{diag}$ describes the difference between the diagonal energy shifts of components 1 and 2. The first term in equation 2 is the midpoint between the excited state energies of the components as influenced by their Van der Waals interactions in space. The second term is the splitting energy, in this case a function of the difference in transition energies of the two individual units as well as the coupling term V, itself a function of the interaction of the excited states of the individual components with each other. An estimate of the coupling term V can be derived from the experimentally determined parameters of the compounds in this work by taking the difference of the transition energies of the cruciform excited states and solving for V:

$$V = \frac{\sqrt{\left(\Delta E_{-}^{(cruc)} - \Delta E_{+}^{(cruc)}\right)^2 - \left(E_{eg}^{(eth)} - E_{eg}^{(vin)}\right)^2}}{4} \qquad (3)$$

where $\Delta E_{\pm}^{(cruc)}$ are the 0-0 transition energies of the exciton-like transitions of the cruciform compounds, the ethynyl and vinyl fragments have taken the place of components 1 and 2 in equation 2, and ΔV^{diag} has been neglected, a common assumption in such cases.{ferguson 1986} Once the coupling term V is known, the wavefunction mixing coefficients (cos(γ/2) and sin(γ/2) for the excitonic states in these cruciforms may be calculated from the equation describing the exciton state wavefunctions $\Psi_{\pm}$ of an exciton with non-degenerate components:{ferguson 1986}

$$\begin{aligned} \Psi_{+} &= \cos(\gamma/2)\psi_e^{(eth)}\psi_g^{(vin)} + \sin(\gamma/2)\psi_g^{(eth)}\psi_e^{(vin)} \\ \Psi_{-} &= \sin(\gamma/2)\psi_e^{(eth)}\psi_g^{(vin)} - \cos(\gamma/2)\psi_g^{(eth)}\psi_e^{(vin)} \end{aligned} \qquad (4)$$

where

$$\gamma = \arctan\left(\frac{2V}{E_{eg}^{(eth)} - E_{eg}^{(vin)}}\right) \tag{5}$$

Exciton analysis of cruciforms without D/A substituent pattern. To obtain the 0-0 energies for the transitions in the spectra of compounds **11** - **14**, the 1PA spectroscopic data were analyzed using a Franck-Condon (FC) bandshape analysis{herzberg 1950; parson 2007} based on equation 6:

$$\varepsilon(E) = \sum_{\upsilon''=0}^{m} \varepsilon_{0-0} \frac{S^{\upsilon''}}{\upsilon''!} \exp\left(-\frac{(E - E_{0-0} - \upsilon'' E_{vib})^2}{\Gamma^2}\right) \tag{6}$$

Equation 6 expresses the extinction coefficient ε(*E*) of a vibronic absorption band as *m*+1 vibronic components of a progression, with each component having a Gaussian line shape. The progression begins with a component at the energy $E_{0\text{-}0}$ between the $\upsilon'' = 0$ vibrational level in the electronic ground state *g* and the $\upsilon' = 0$ vibrational level in the electronic excited state *e*, and ends with the component at energy $E_{0\text{-}m}$ between the $\upsilon'' = 0$ vibrational level in *g* and the $\upsilon' = m$ vibrational level in *e*. Each component is assumed to have the same linewidth Γ and is separated from its neighboring components by the vibrational frequency ω_v corresponding to the energy E_{vib}. The Supporting Information contains a more detailed description of the bandshape fitting method. The results of the Franck-Condon fitting for compounds **11**-**14** are shown in Figure 7 and Table 2.

The spectra of linear model compounds **11** and **12** are each reasonably modeled by an electronic transition with a single vibrational mode FC progression with each line having a Gaussian bandshape, for which a linewidth of 0.1 eV led to good agreement with the observed spectra. The spectrum of the cruciform **13** is decomposed into two bands: a low-energy band with a FC bandshape similar to that of **12**, and a high-energy

band at a similar energy to that of **11,** although with a rather different overall bandshape. The spectrum of cruciform **14** has two bands with shapes very similar to those of **13**, although they are red-shifted by 0.5 eV (high-energy band) and 0.4 eV (low-energy band), which suggests that adding identical π-donor groups at all four terminal phenyl groups in the cruciform structure does not have a large impact on the nature of the inter-arm coupling, but destabilizes the HOMO of the cruciform as expected. Generally the bandshapes are consistent with moderate changes in geometry upon excitation as evidenced by the Huang-Rhys factors (~ 1.0 – 1.6), and damping widths of ~0.1 eV. The fitting of the high-energy band of **13** and **14** with Γ constrained to assume a value of 0.1 eV was not definitive in terms of the vibrational frequency, Huang-Rhys factor or bandwidth. An alternative set of values obtained from a fit performed with Γ as an unconstrained fitting parameter also fit this peak well, but gave rise to a much larger vibrational frequency, lower Huang-Rhys factor and an unusually large bandwidth. The values of the 0-0 energies for the low-energy and high-energy bands were quite consistent between the different fittings. The residual intensity between the two FC band fittings and the observed spectra of **13** and **14** were fairly small except in the higher energy region, which indicates the presence of another electronic absorption band. In the case of **15**, in addition to a deviation at high energy, there is a significant area of residual intensity in between the main bands in the spectrum. As we will discuss below, the intensity of this residual band becomes more pronounced when there is a greater disparity in the electron donor and acceptor character of the terminal groups of the two arms.

With the $E_{0\text{-}0}$ values for all transitions in the spectra of **11**-**14** obtained from the FC analysis along with the $E_{0\text{-}0}$ value for **1a** from the literature,{pond 2002} which is at 2.87

eV, and the lowest-energy feature of **2a**,{nguyen 1994} which is at 3.18 eV and is a reasonable approximation for $E_{0\text{-}0}$ of **2a**, we have calculated for **13** and **14** the ππ* excitonic coupling term V and the wavefunction mixing coefficient, sin(γ/2), using equations 3 and 4. The values of V for **13** and **14** are 0.23 eV and 0.16 eV, respectively. Apparently, the symmetrical tetra-donor substitution leads to a smaller magnitude of the effective excitonic interaction energy and the wavefunction mixing. The square of the sin(γ/2) wavefunction mixing coefficient of the ethynyl arm in the low-energy exciton state is 0.20 for **13** and is 0.15 for **14**, showing that there is significant mixing of the π* excited states in both cases.

Charge transfer interactions in cruciforms with D/A substituent pattern. The low-energy band in the electronic spectra of **15**-**20** are broader than those of **13** and **14** and for **16**-**20** there is clear evidence for a splitting of the low-energy band which is too large to be due to a vibrational mode. We take this as evidence for a distinct excitonic interaction, relative to that in **13** and **14**, which is correlated with the presence of electron deficient terminal groups on the ethynyl arms; i.e. that this splitting is associated with a coupling of charge transfer transitions in the D/A cruciforms. In the cases of the D/A substituted cruciforms **16**-**20**, as the degree of intramolecular charge transfer increases, the overall bandshape of the low-energy band evolves with a red-shift of the band edge and a redistribution of oscillator strength from the lower-energy component (sub-band 1) to the higher-energy component (sub-band 2) of this band. It should be noted that both the high-energy band (at approximately 340-350 nm) and the width of the low-energy band (at approximately 430 nm) are unique to D/A substituted cruciforms with non-degenerate

conjugation in ethynyl and vinyl arms, as compared to those reported in the literature for **4** and **6** degenerate ethynyl or vinyl arms. This two-band structure is also not present in linear bis(dimethylaminostyryl)benzene compounds with acceptors substituted directly on the central phenyl ring; a comparison may be made of cruciform **19** to the linear compound **1b**, which is analogous to **19** but with the cyano groups directly on the central phenyl ring, lacking the phenylethynyl linkers. The absorption spectrum of **1b**{pond 2002} shows only one main electronic transition in the 1PA spectrum, lacking another transition corresponding to the higher-lying transition in **19**; the spectrum of **1b** is also narrower and lacks the low-energy shoulder found in **19.**

In **20**, which has the strongest acceptor group (-NO_2), sub-band 2 is the dominant component of the low-energy band, whereas for the other acceptor substituted cruciforms and **15**, sub-band 1 is more intense. This trend may be explained by a greater contribution to the low-energy band from coupled charge-transfer states as the acceptor strength is increased. This is illustrated for the limiting case of a strong charge-transfer contribution in Figure 8: in this case, charge transfer excitations from the donors to the ortho-coupled acceptors are considered. Each charge-transfer excitation is assigned a transition dipole μ_i^{CT}. Since the charge-transfer transition dipoles are energetically degenerate and anti-parallel, the excitonic interaction between the charge-transfer transitions may be described more simply than for the case of electronically nondegenerate component units discussed earlier. For an exciton composed of anti-parallel, nondegenerate component units, the excited state energy of each unit E_e^0 is shifted by the diagonal energy shift V_{eg}^{diag}, and the energies of the exciton excited states, $E_\pm$, are split by $2V$ from this stabilized energy.

$$E_{\pm} = E_e^{\,0} + V_{eg}^{\,diag} \pm V \qquad (7)$$

As earlier, V is the coupling term between the excited states of the component units; however, in this case the splitting energy is simply equal to V. The transition to the higher energy exciton state ψ_-^{CT} is one-photon allowed, while the transition to the lower energy exciton state ψ_+^{CT} is one-photon forbidden.{kasha 1965}

While this interpretation provides a reasonable explanation of the 1PA spectrum of **20**, the intensity distributions of the sub-bands of compounds **15**-**19** (with weak to moderate acceptor groups) are not what would be expected from an antiparallel arrangement of degenerate charge-transfer chromophore units. The spectrum of compound **15**, with the lowest acceptor strength (an unsubstituted phenyl), appears to be similar to the spectra of **13** and **14**, which we described above using a $\pi\pi^*$ exciton picture. There is one cruciform band near the transition energy of the ethynyl model compound **11**, and one cruciform band (sub-band 1) near the transition energy of the styryl model compound **1a**. The low-energy side of the low-energy cruciform band can be fit reasonably well to a FC distribution very similar to that of model compound **1a**{pond 2002} (see Table 2 for the parameters of the fit of the low energy side of the spectrum of **15**). Figure 9 shows that there is substantial residual intensity in between the low-energy and high-energy bands of the cruciform, upon subtraction of the two fitted FC bandshapes, which indicates the presence of an additional electronic band. We attribute this band to a higher energy sub-band (sub-band 2) as described for the D/A cruciform **16**-**20**.

Upon progressing to cruciforms with higher acceptor strengths in compounds **16**-**19**, the spectra of the low-energy band become increasingly similar to that of **20**, in which

the coupling of the CT states dominates the low-energy band. The intensity distributions for intermediate cruciforms suggest that there are significant contributions of the ππ* exciton character (a lower energy band with significant oscillator strength) and CT exciton character (low oscillator strength in sub-band 1 and high intensity in sub-band 2). Even though the composition of the low-energy bands is complex we employ a simple splitting analysis to estimate the coupling term V_{CT} for the CT exciton from the splitting of the sub-bands. A modified FC analysis (described in the Supporting Information) was applied to the low-energy band, to obtain estimates of $E_{0\text{-}0}$ for each sub-band.

The results of the modified FC fits are given in Figure 9 and Table 3. The modified fitting procedure gave spectra in reasonably good agreement with the experimental spectra. As shown in Table 3, the values of $\Delta E_{0\text{-}0}$, the gap between the $E_{0\text{-}0}$ energies of sub-bands 1 and 2, were used to estimate the charge-transfer coupling term V_{CT} for the D/A substituted cruciforms by the relationship $\Delta E_{0\text{-}0} = 2\ V_{CT}$. The value of V_{CT} increases with increasing acceptor strength, as does the ratio of the amplitudes $\varepsilon_{0\text{-}0}(1):\varepsilon_{0\text{-}0}(2)$. These trends indicate both stronger coupling between the CT transitions as well as the stronger influence of the coupled CT transitions on the overall character of the low-energy absorption band.

A coupling energy for the ππ* states may also be estimated for **15**-**20**. Using the centroid of the two sub-bands as ΔE_{+}, and the lowest energy features reported{nguyen 1994} for acceptor substituted bis(phenylethynyl)benzenes **2b**-**2d**, which are 3.58, 3.46, and 3.26 eV, respectively, the ππ* coupling energies V of compounds **15**, **17**, **19** and **20** were calculated to be 0.096, 0.144, 0.195 and 0.268 eV, respectively. This increase of V suggests an increase of electronic overlap between the ππ* excited states of the two arms

with increasing acceptor strength. The corresponding ππ* mixing coefficients $\sin^2(\gamma/2)$ are 0.017, 0.036, 0.082 and 0.20. The coupling terms and mixing coefficients of **13**-**15**, **17**, **19** and **20** are shown graphically in Figure 10.

2PA spectra of linear compounds and cruciforms without D/A substituent pattern. The $\lambda_{max}^{(2)}$ and δ_{max} of **12** are close to the well-characterized and extremely similar molecule BMSB[86,87] (in cyclohexane). The larger HOMO-LUMO gap of **11** causes its 2PA peak to be shifted hypsochromically (relative to **12** and BMSB) too far to be observable with the set-up used. Since the $\lambda_{max}^{(2)}$ of **13** was also outside of the set-up measurement range, it is not possible to determine if the 2PA excited states of the component arms of **13** interact in the same way as the 1PA excited states. Over the wavelength range studied, the shape of the 2PA spectrum of **13** is relatively similar to that of the sum of **11** and **12**, although the magnitude of δ is less for **13** than for the sum of **11** and **12** between 550 – 600 nm. This suggests that there is relatively little coupling between the 2PA excited states of the linear components of **13**, and the lower magnitude of the 2PA spectrum of **13** than the sum of **11** and **12** is consistent with the exciton description of Rumi et al.{rumi JPCC 2008}

It is possible to gain more insight into the coupling of the 2PA excited states by examining **14**. The δ_{max} of **14** is 1200 GM at 700 nm, while there is a shoulder with δ = ~550 GM at approximately 750 nm, in distinction to the 2PA spectra of **3** and **5**, each of which have one peak and no obvious shoulder. We attribute this to the differing conjugated arms in **14** as opposed to the identical conjugated arms in **3** and **5**. Equations

analogous to equations 7 and 2 may be written for the $g \rightarrow e'$ 2PA transition energies of excitons composed of identical (equation 8) or nonidentical (equation 9) units:

$$E_{(\pm)'} = E^{0}_{e'} + V^{diag}_{e'g} \pm V' \tag{8}$$

$$E_{(\pm)'} = \frac{E^{(1)'}_{e'} + E^{(2)'}_{e'}}{2} \pm \frac{\sqrt{(E^{(1)}_{e'g} - E^{(2)}_{e'g} + \Delta V^{diag''})^2 + 4(V')^2}}{2} \tag{9}$$

In equation 9, $E_{e'g}^{(1)}$ is the $g \rightarrow e'$ transition energy of component 1, $E_{e'g}^{(2)}$ is the $g \rightarrow e'$ transition energy of component 2, and $\Delta V^{diag''} = V_{e'g}^{diag} - V_{ge'}^{diag}$. Rumi et al.{rumi jpcc 2008} showed that the splitting energy for 2PA transitions in cruciforms such as **3** composed of identical units is near zero, since the splitting energy is equal to the coupling term V'. As V' is zero or near zero for 1PA-forbidden transitions to the e' state of a cruciform composed of identical arms, the small splitting energy leads to only one apparent 2PA band. In the case of differing units here, the splitting energy is a function not only of V but of $E_{e'g}^{(eth)} - E_{e'g}^{(vin)}$ as well. In fact, if both $\Delta V^{diag''}$ and V' are neglected, the splitting term in equation 3.21 is simply half of the quantity $E_{e'g}^{(eth)} - E_{e'g}^{(vin)}$. For a qualitative comparison, we refer to the 2PA spectra of **1c**[40,88] and **2e.**[140] While the donor groups of these chromophores are not identical to those of **14**, the $\lambda_{max}^{(2)}$ of **1c** is shifted by only 0.04 eV from that of compound **1a**. To a first order approximation, we assume that a similar shift is present between the $\lambda_{max}^{(2)}$ of **2e** and that of **2a**, and use the difference between the peak 2PA trantition energies of **1c** and **2e** to approximate $E_{e'g}^{(eth)} - E_{e'g}^{(vin)}$ for **2a** and **1a**. The peak 2PA transition energy of **2e** is at 3.56 eV, while the peak 2PA transition energy of **1c** is at 3.33 eV, resulting in a splitting energy of 0.115 eV. Using the wavelengths of the 2PA peak and shoulder of **14** to approximate the cruciform

"excitonic" 2PA transition energies 3.54 and 3.30 eV, the actual splitting of the features in the spectrum of **14** is 0.12 eV from the center energy, consistent with the approximated splitting energy derived from the $\lambda_{max}^{(2)}$ of **1c** and **2e**. This strongly suggests that in the absence of strong coupling of the 2PA excited states of the non-degenerately conjugated linear arms of cruciforms such as **14**, there are two cruciform "exciton" 2PA transitions attributable to the differing linear arms, with little wavefunction mixing. This interpretation is consistent with previous work indicating low mixing of 2PA excited states in cruciforms with degenerate arms{rumi jpcc 2008} and in paracyclophane-linked linear chromophores.{bartholomew 2004}

2PA spectra of cruciforms with D/A substituent pattern. The 2PA spectra of the D/A-substituted cruciforms **15**-**20** all show evidence of more than one 2PA transition in the range investigated, a main peak between 770-830 nm and a secondary band at approximately 950 nm. These transitions correlate with the two sub-bands calculated in the modified FC fitting (see Figure 9). Specifically, the strongest 2PA band corresponds to sub-band 2, while the weaker 2PA band correlates with sub-band 1, for compounds **15**-**19**. As the acceptor strength increases from **15** to **19**, the δ_{max} and the peak δ of the lower energy 2PA band increase in magnitude (see Figure 5), while $\lambda_{max}^{(2)}$ shows a slight red-shift (see Table 3). As the charge-transfer character of the lower energy states grows with increasing acceptor strength, the magnitude of the lower energy 2PA bands increase, as has been observed for quasi-linear conjugated donor-acceptor-donor systems.{albota 1998} On the other hand, **20**, with $-NO_2$ acceptors, exhibits a substantially broadened and blue shifted 2PA spectrum with both a lower δ_{max} and a blue-shifted $\lambda_{max}^{(2)}$ compared to

19, which has -CN acceptors. Compounds **4**{rumi jpcc 2008; rumi spie 2008} and **6**{slepkov 2006; slepkov 2005}also display relatively broad 2PA spectra, although the low-energy 2PA transitions of both are slightly redshifted from the energy of their main 1PA transitions. Unlike **4**, **6** and cruciforms **15** - **19**, the peaks of the 2PA spectrum of **20** are blue shifted relative the to the 1PA peaks of the sub-bands. This may be due to the presence of overlapping additional bands that give apparent shifts in the positions of the maxima, possibly including the 2PA band from the ππ* excited state of the ethynyl arm. The CT exciton model would predict that the lower energy excited state would be of A_g symmetry and the upper state B_u, consistent with the relative intensities of the 1PA bands, and would indicate that sub-band 2 would show little or no 2PA activity. With the lowering of the energy of the ππ* excited state of the ethynyl arm upon $–NO_2$ substitution there may be additional state mixings of CT and ππ* states that have not been accounted for by the independent exciton models described above and may result in redistribution of two-photon intensity into higher energy states. Further theoretical studies will be needed to explain the 2PA spectrum of **20**.

The δ_{max} of **15** (740 GM) and **19** (950 GM) show significant reductions from their respective linear bis(styryl)benzene model compounds **1a** (995 GM) and **1b** (1750 GM). There is also a bathochromic shift of the $\lambda_{max}^{(2)}$ of cruciform **15** (770 nm) with respect to the peak of the linear compound **1a** (730 nm); there is no such bathochromic shift in the $\lambda_{max}^{(2)}$ of **19** relative to **1b** ($\lambda_{max}^{(2)}$ = 830 nm for both). This indicates the cruciform architecture with both double- and triple-bond arms does not inherently lead to enhanced values of δ_{max} (for the all-parallel polarization tensor component) relative to similar linear compounds that have identical donor and acceptor substituents but lack a phenylene-

ethynylene bridge to the electron acceptor. The D/A cruciform motif does provide some ability to tune 2PA band positions and bandwidths, which can be useful for some applications.

Summary and assignment of state symmetries. The results and modeling of the one and two photon absorption spectroscopy of the cruciforms examined lead to the following overall description: for the unsubstituted or tetra-donor substituted cruciforms, which do not possess substantial intramolecular charge-transfer character, coupling of non-identically conjugated linear units results in some mixing of the ππ* excited states. The interaction of the linear units in the cruciform produces two cruciform excited states with increased splitting over the splitting of the excited states of the independent units. For the cruciform with strong dialkylamino donors and nitro acceptors **20**, there is strong mixing of pairs of charge-transfer states associated with different CT pathways, which gives rise to a strong splitting of the low-energy 1PA band into a low energy weak band (A_g excited state) and a much stronger band (B_u excited state) at higher energy. In the cruciforms with weak to moderate acceptor strength, **15**-**19**, the transitions appear to be of mixed ππ* and CT exciton character and with the CT character of the lower energy states (that correlate with the donor substituted vinyl arm ππ* state in the limit of weak acceptor strength) increasing as the acceptor strength is increased. The high-energy band (that correlates with the bis(phenylethynyl)benzene arm ππ* excited state) is stabilized by acceptor substitution and appears to be less influenced by the CT interaction.

The trends in the evolution of the state energies of the compounds in this study is illustrated in Figure 11. Assignments of the excited states were made based on the

observed locations of 1PA and 2PA bands and symmetry selection rules for the D_{2h} point group. In centrosymmetric chromophores such as these cruciforms, 1PA transitions from the ground $1A_g$ state are allowed to excited states with different parity, such as B_u states; 2PA transitions are allowed to higher-lying excited states with the same A_g symmetry. Thus in Figure 11, the energies of the $1B_u$ and $2B_u$ states are derived from the peaks in the 1PA spectra, while the energies of the $2A_g$, $3A_g$ and $4A_g$ states are derived from the 2PA peaks. When moving from the linear **11** and **12** to the cruciform **13**, the most notable change is the inferred lowering of the $2A_g$ state from 4.3 eV to ~4 eV, while the remainder of the state energies do not change greatly. The D/A cruciform **15** shows a significant lowering of both the double-bond arm derived $1B_u$ and $2A_g$ states, while the triple-bond arm derived $2B_u$ and $3A_g$ states show relatively little change. Increasing the acceptor group strength in **16**-**19** results in the further lowering of both the $1B_u$ and $2B_u$ state (δ_{max}). In **20** the $2B_u$ state is at the lowest energy of any of the cruciforms, while the highest-energy 2PA state ($4A_g$) can be identified.

Conclusions

We have reported the linear absorption, fluorescence and two-photon excited fluorescence properties of eight cruciforms with one bis(styryl)benzene and one bis(phenylethynyl)benzene arm as well as of two linear model compounds representing each non-degenerate arm. The linear- and two-photon absorption spectra of the cruciform with no electron donor or acceptor groups or a cruciform with identical electron-donor substituents on each arm are explained within a $\pi\pi^*$ exciton framework. The spectra of the cruciforms substituted with electron-donors on the bis(styryl)benzene arm and

electron-acceptors on the bis(phenylethynyl)benzene arm are explained as a superposition of a weakly-mixed ππ* exciton with an intramolecular H-aggregate exciton associated with degenerate charge-transfer transitions between the electron-donors and electron-acceptors. The two-photon absorption cross-sections reported for our cruciforms are on the same order of magnitude as those reported for similar cruciform compounds with degenerate arms; {rumi jpcc 2008; rumi spie 2008; slepkov 2006; slepkov 2005} the incidence and systematic variation in the strength of a secondary 2PA band at 950 nm due to a 1PA forbidden transition is reported here for the first time.

The composite ππ* and CT exciton model description for conjugated cruciforms with non-degenerate arms provides useful insight into the nature of the electronic transitions in the visible and near-IR range and may be useful in the design of two-photon absorption based sensing chromophores that can take advantage of the shift from weak mixing between arms to strongly coupled charge-transfer transitions involving both arms. While the use of strong donor groups and strong acceptor groups might be expected to provide the strongest and most red-shifted 2PA peaks, these objectives would both be best achieved with strong donors and moderate acceptors.

Scheme 1: Synthetic pathway providing access to cruciform chromophores **13-20**.

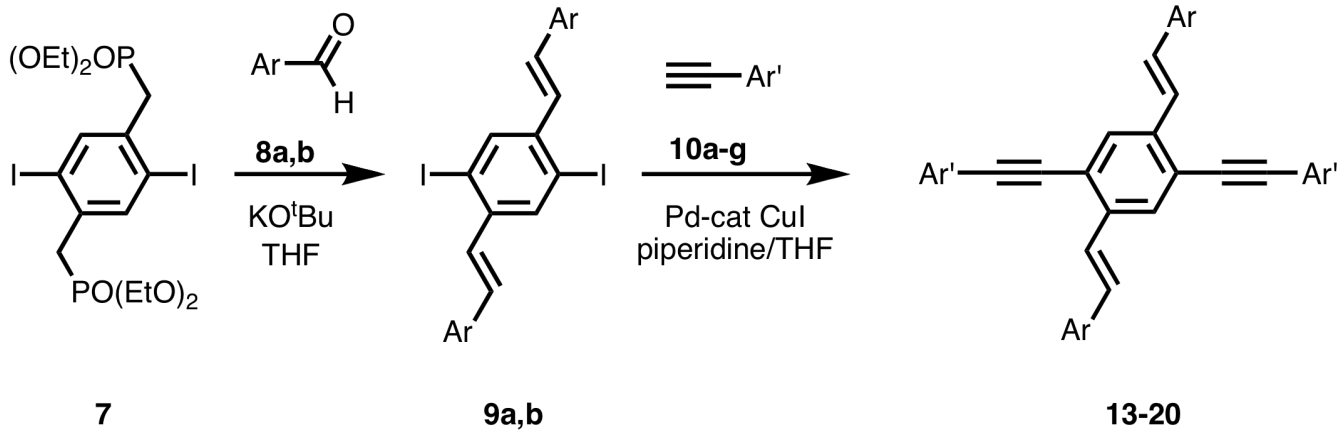

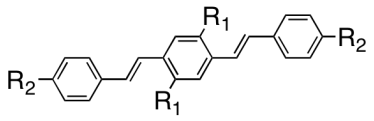

1a: R_1 = H; R_2 = NBu_2
1b: R_1 = CN; R_2 = NBu_2
1c: R_1 = H; R_2 = N(Ph)((3-CH_3)-Ph)

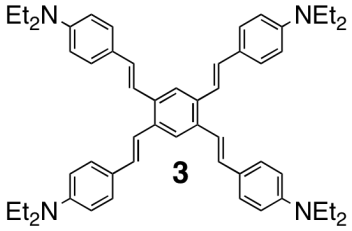

3

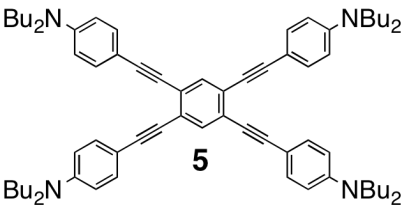

5

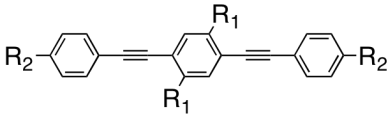

2a: R_1 = H; R_2 = NBu_2
2b: R_1 = H; R_2 = CF_3
2c: R_1 = H; R_2 = CN
2d: R_1 = H; R_2 = NO_2
2e: R_1 = CH3; R_2 = N((4-CH_3O-)Ph)$_2$

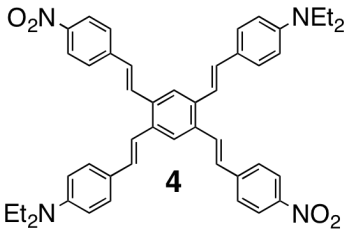

4

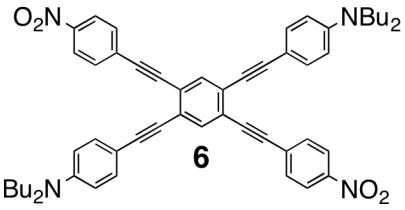

6

Figure 1: Structures of compounds reported in the literature and used as examples and comparisons in the present work. Compounds **1a** and **1b** were reported in Pond;{Pond 2002} compound **1c** in Rumi{Rumi 2000}; compounds **2a**-**2d** in Nguyen{Nguyen 1994} and **2e** in Strehmel.{strehmel 2005} Compounds **3** and **4** were reported in Rumi.{Rumi JPCC 2008; Rumi SPIE 2008} Compounds **5** and **6** were reported in Slepkov.{Slepkov 2006; slepkov 2005}

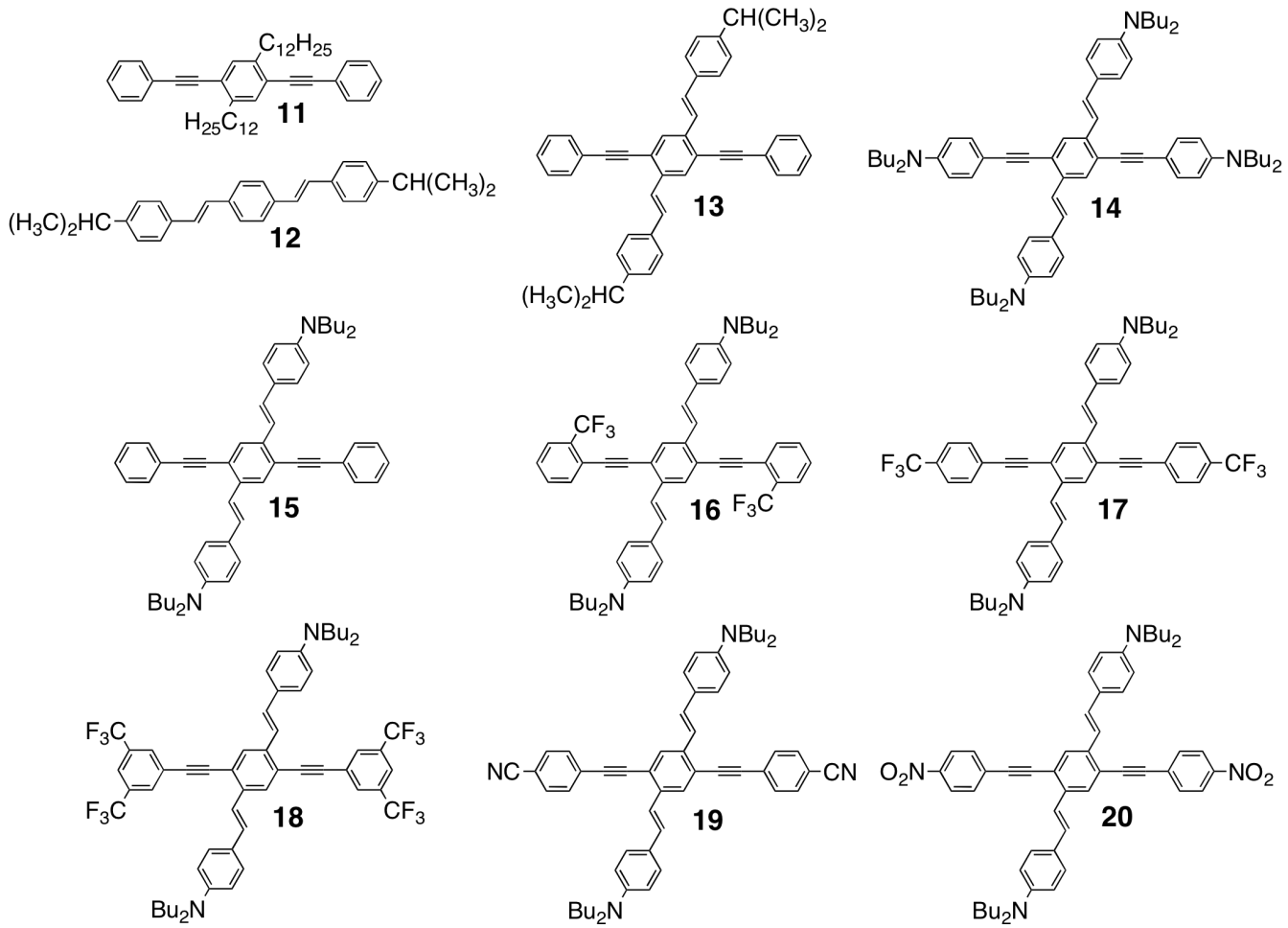

Figure 2. Structures of compounds **11-20** examined in this paper.

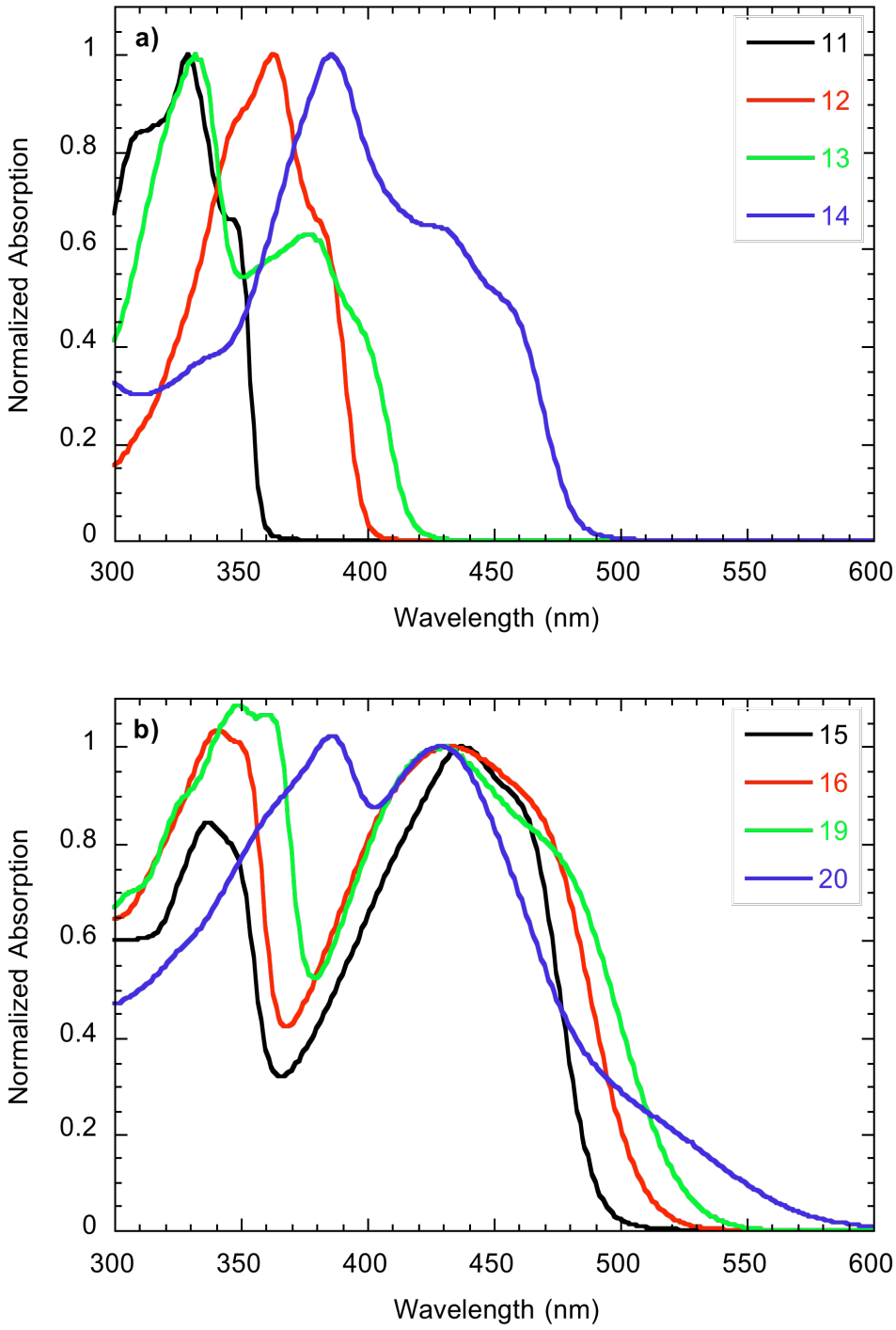

Figure 3: UV/visible absorption spectra of selected chromophores: **a)** Spectra for the linear model compounds (**11** and **12**) and the cruciform with no donor substituents (**13**) and four donor sustituents (**14**). **b)** Spectra for cruciforms with electron-donor groups on the bis(styryl)phenylene arm and either no substituents (**15**) or electron acceptors on the bis(phenylethynyl)phenylene arm (**16**, **19** and **20**). [The UV/vis spectra of **17** and **18,** which are very similar to those of **16** and **19**, respectively, are included in the Supporting Information.]

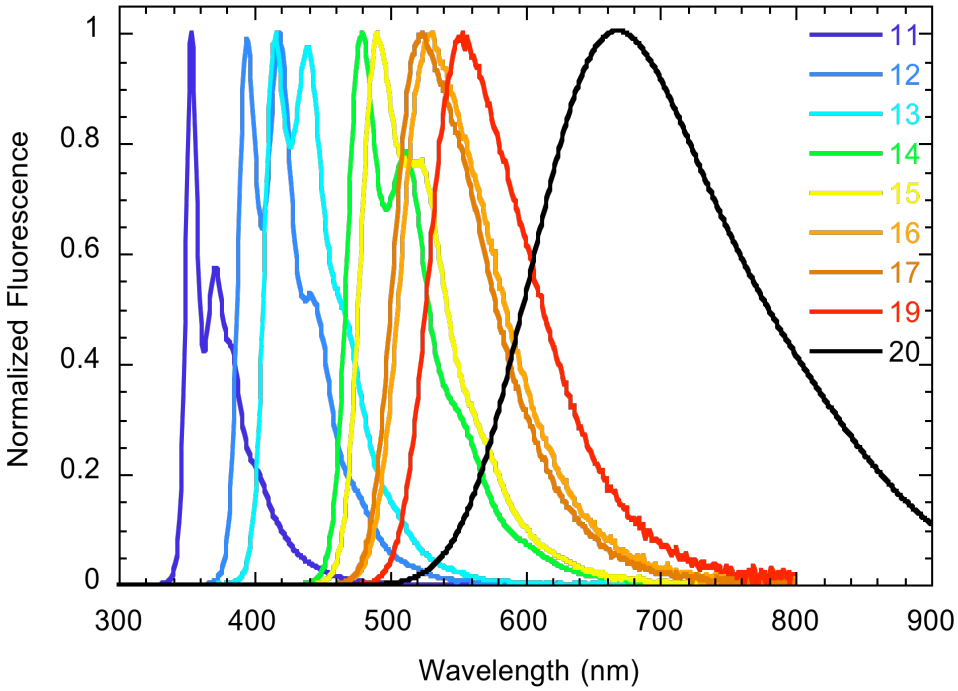

Figure 4: Fluorescence spectra of the linear model compounds **11** and **12** and cruciform compounds **13**-**17**, **19**, **20**. The spectrum of **18** is nearly identical to that of **19** and was omitted here for clarity(see Supporting Information). Note that the spectrum of **20** is a model consisting of a single Gaussian function fit by linear-least-squares to the non-noisy part of the experimental spectrum as collected on the fluorimeter (see Supporting Information).

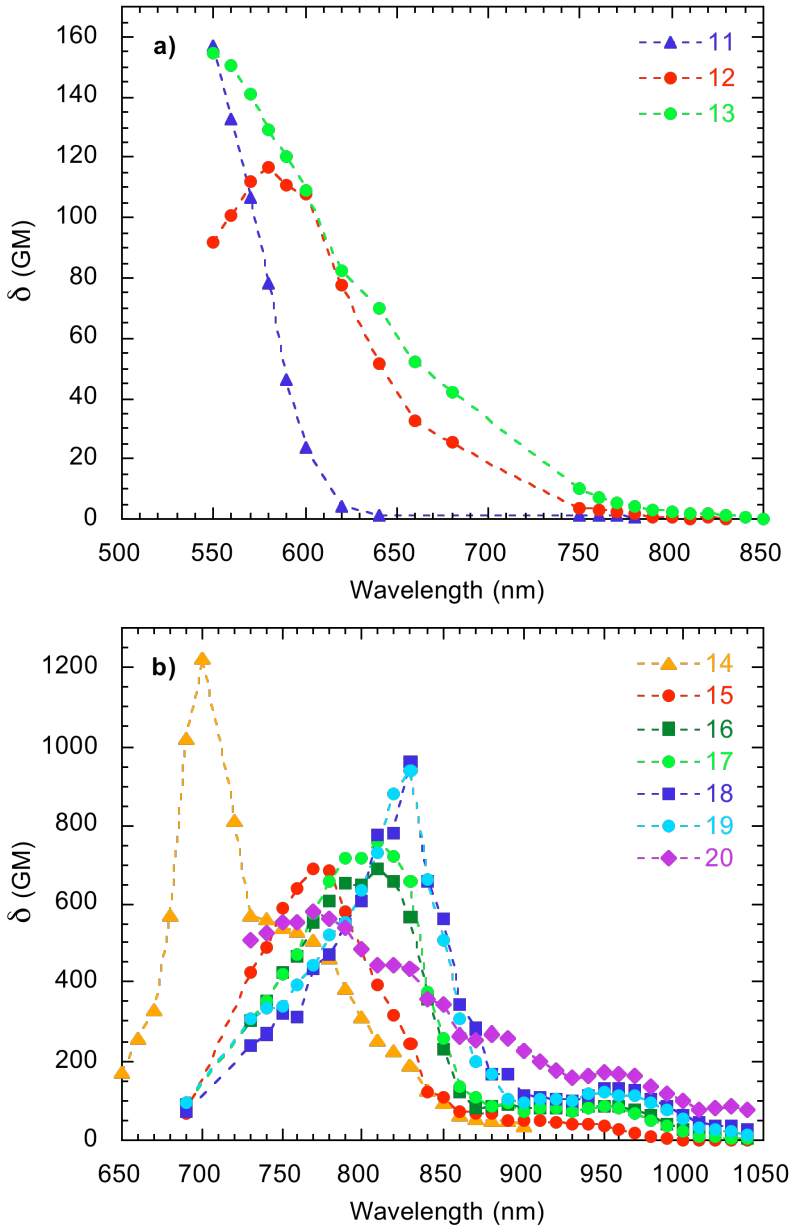

Figure 5: Two-photon absorption spectra of selected compounds. In all cases, the lines shown are not fits but are intended as guides for the eye. Shown in **a)** is the change in 2PA spectrum upon transitioning from the linear model compounds **11** and **12** to the unsubstituted cruciform **13**. In **b)** are 2PA plots of substituted cruciforms.

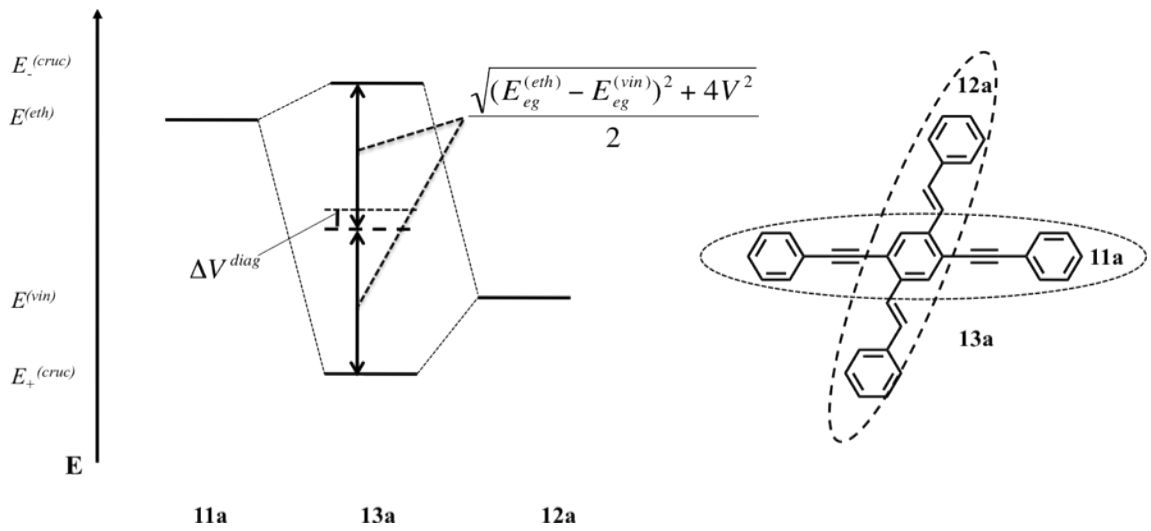

Figure 6: A diagram depicting the electronic excited states of the linear compounds **11a** and **12a** (similar to **11** and **12**, with alkyl groups omitted for clarity) and the joint cruciform molecular orbitals formed by their exciton mixing in the cruciform compound **13a**.

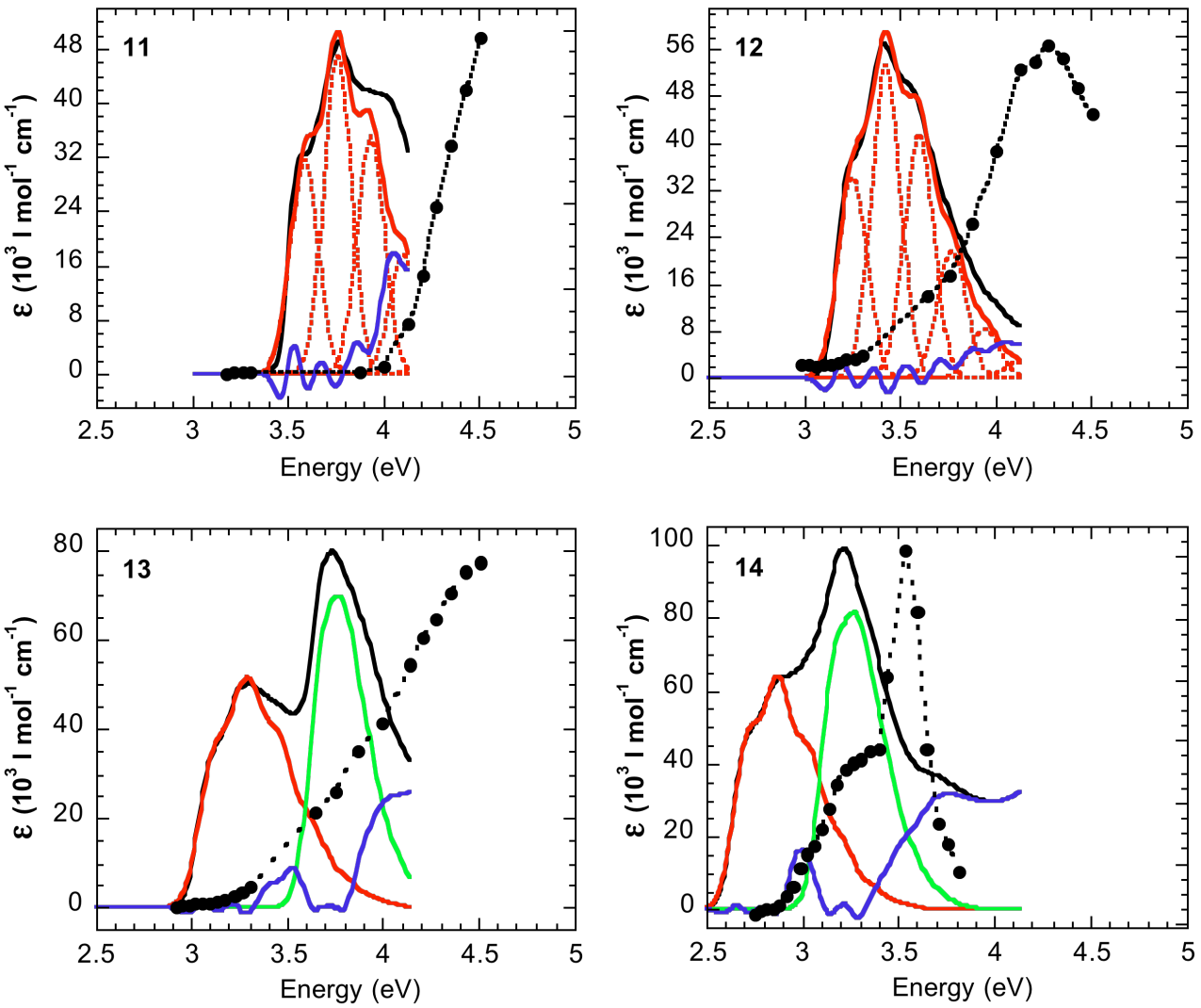

Figure 7: 1PA (black lines) and 2PA (black circles) spectra plotted as a function of transition energy, and results of the Franck-Condon bandshape analysis of the 1PA band for cmpounds **11**-**14**. For **11** and **12**, red dashed lines represent the six individual components of the Franck-Condon progression calculated. Individual Franck-Condon components are not included for **13** and **14** for the sake of clarity. In all plots, bold red solid lines represent the sum of the components of the Franck-Condon progression of the lowest-energy band. For **13** and **14**, green lines represent the total Franck-Condon fit of the higher energy component, while the blue lines are the total residuals (i.e. experimental spectrum – (total fit of lower-energy band) + (total fit of higher-energy band)).

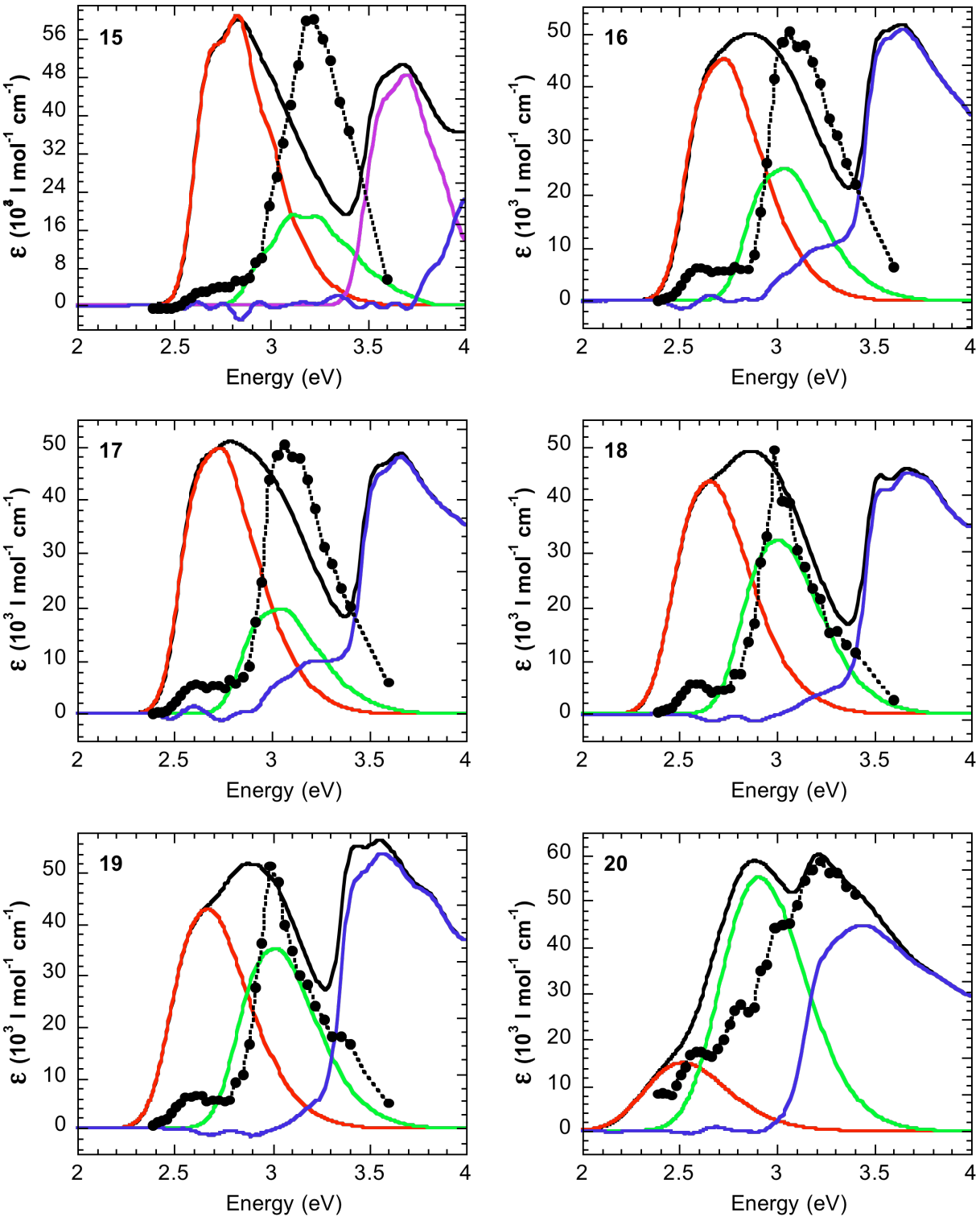

Figure 8: 1PA (black lines) and 2PA (black circles) spectra plotted as a function of transition energy, and results of the Franck-Condon bandshape analyses of compounds **15**-**20**. The plot for **15** displays the sums of the six vibronic components derived from Franck-Condon fits of the lowest energy band (red line), the middle band (green line) and phenylethynyl-derived band (purple line) along with the total

residual (blue line). The plots for **16**-**20** display the results of the modified Franck-Condon (described in the Discussion): sub-band 1 (red line), sub-band 2 (green line), and residual (blue line).

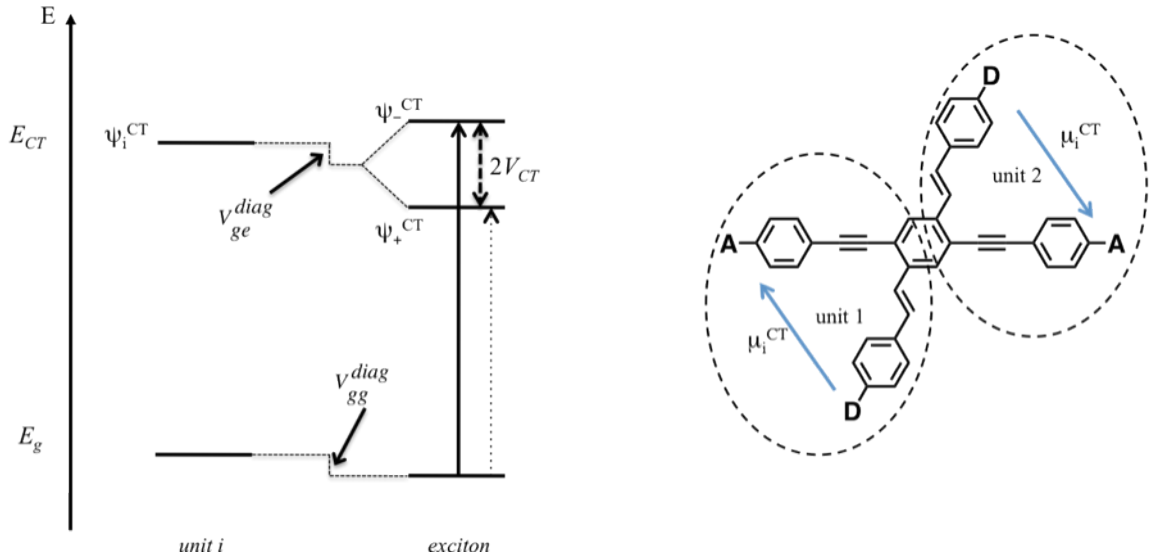

Figure 9: A diagram of the charge-transfer transitions in identical V-shaped components of D/A-substituted cruciforms. The energy-level diagram on the left is typical of the splitting of the exciton transitions in an H-aggregate. The allowed transition is represented by a solid arrow from the exciton ground state to ψ_-^{CT}, while the forbidden transition is represented by a light dashed arrow from the exciton ground state to ψ_+^{CT}.

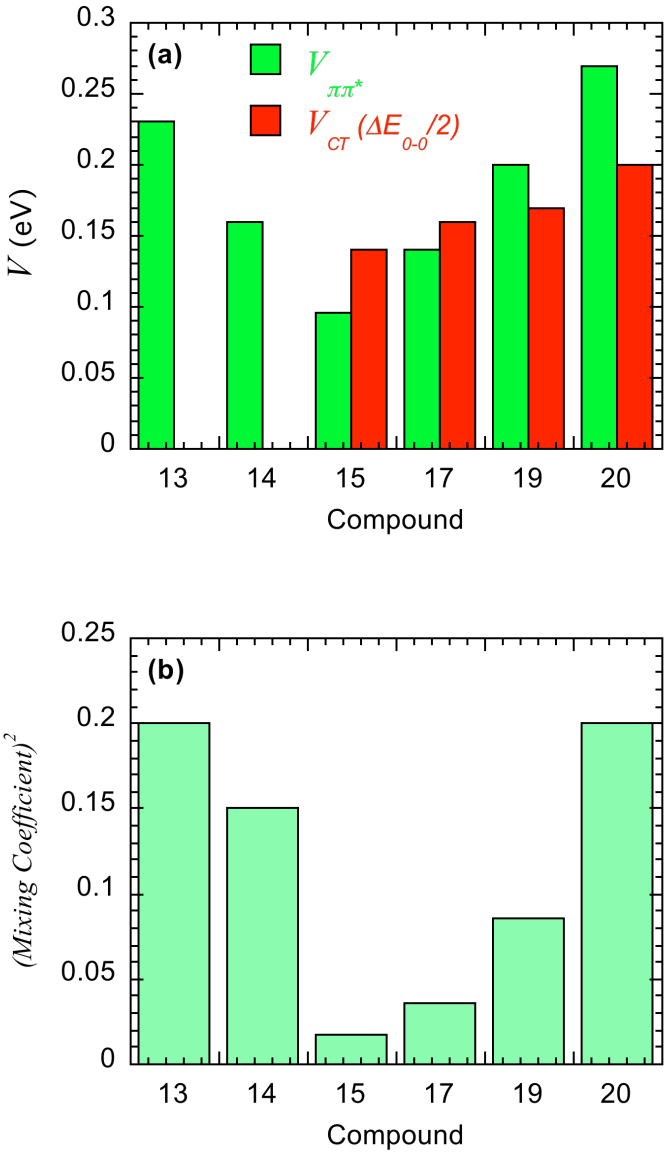

Figure 10. Plots of the coupling terms and mixing coefficients for selected cruciforms. For the ππ* mixing, the coefficient shown is the sin(γ/2) term. For the charge-transfer transition mixing, the coefficient is the value given by theory, $2^{-1/2}$.

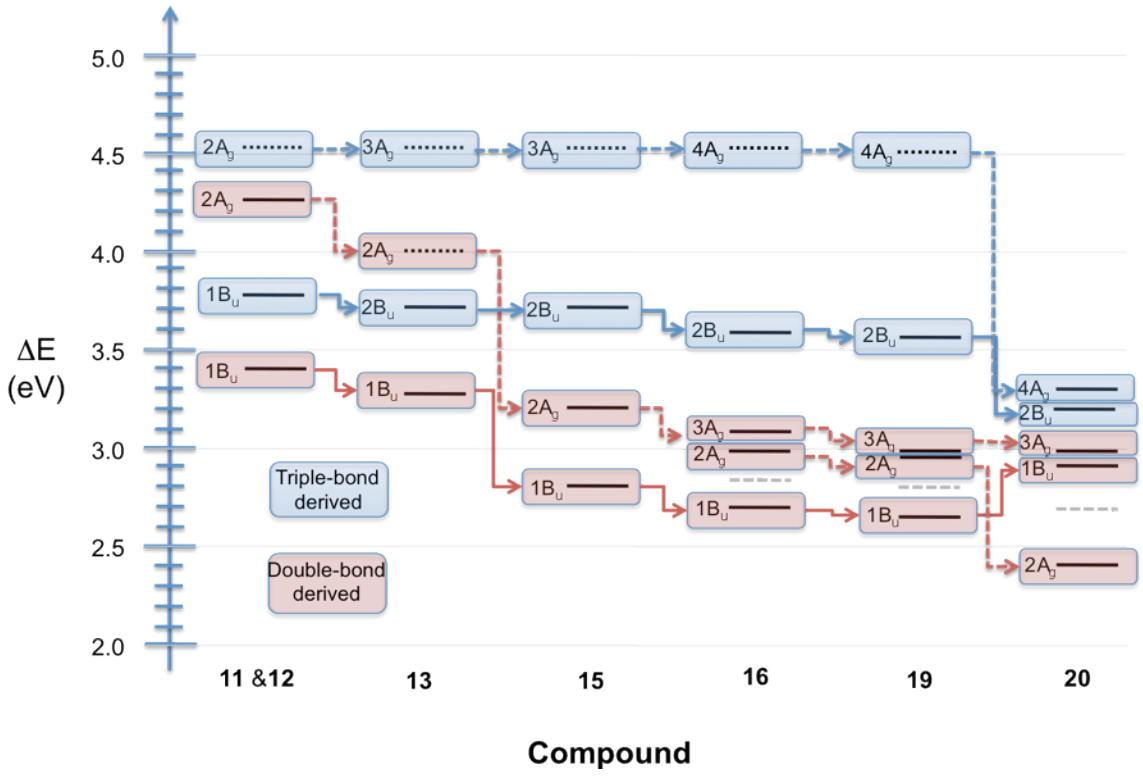

Figure 11: State energy diagram of selected linear model and cruciform compounds. The ΔE axis represents the peak energy of electronic transitions between the ground state and excited states in the compounds. Blue highlighted states are those localized on the bis(phenylethynyl)benzene arm, while red highlighted states are those localized on the bis(styryl)benzene arm. Solid arrows are used to connect B_u states, and dashed arrows to connect A_g states. Dashed lines are used to describe states whose energies were not indentified in the reported work.

Table 1. Experimental Linear and Two-Photon Spectroscopic Properties of Chromophores **11** - **20**.

Compound	$\lambda_{max}^{(1)}$ (nm)[a]	$\lambda_{s}^{(1)}$ of shoulder (nm)[b]	ε_{max} (M^{-1} cm^{-1})[c]	$\lambda_{fl}^{(1)}$ (nm)[d]	η_{fl}[e]	$\lambda_{max}^{(2)}$ (nm)[f]	δ_{max} (GM)[g]
11	329	350	49000	354	0.80	550	160
12	363	382	57000	396	0.95	580	120
13	332	400	80000	416	0.79	550	150
14	386	450	99000	480	0.64	700	1200
15	435	460	60000	491	0.66	770	740
16	433	470	50000	529	0.68	820	640
17	441	470	51000	524	0.71	810	730
18	431	475	49000	557	0.70	830	910
19	429	475	52000	554	0.67	830	950
20	430	515	59000	670	0.005	770	580

[a] For **11**-**14**, wavelength of the of the absorption maximum. For **15**-**20**, wavelength of the absorption maximum of the lower-energy band. [b] Approximate wavelength of the lowest-energy feature in the UV/vis absorption spectrum. [c] Molar extinction coefficient at $\lambda_{max}^{(1)}$. [d] Wavelength of the maximum in the fluorescence emission spectrum. [e] Fluorescence quantum yield. Uncertainty in η_{fl} is ± 5%. [f] Maximum of two-photon excited fluorescence excitation spectrum. [g] Peak two-photon cross section (1 GM = 10^{-50} cm^4 s $photon^{-1}$ $molecule^{-1}$). Uncertainty in δ is ± 15%.

Table 2: Parameters of Franck-Condon fitting of Compounds **11**-**15**.(*)

Compound	$\varepsilon_{0\text{-}0}$[c] (l mol^{-1} cm^{-1})	E_{vib} (cm^{-1})[d]	$E_{0\text{-}0}$ (eV)[e]	S[f]	Γ (eV)[g]
11	32,000	1400	3.59	1.49	0.10
12	34,000	1350	3.25	1.57	0.10
13[a] *low-energy band*	31,000	1360	3.12	1.46	0.11
13[a,b] *high-energy band*	49,000 (68,000)	1050 (1500)	3.69 (3.69)	1.04 (0.77)	0.1[h] (0.14)
14[a] *low-energy band*	44,000	1310	2.72	1.32	0.10
14[a,b] *high-energy band*	59,000 (60,000)	1090 (1290)	3.16 (3.19)	1.11 (0.79)	0.1[h] (0.14)
15[a] *low-energy band*	47,000	1290	2.68	1.14	0.10
15[a] *high-energy band*	35,000	1240	3.56	1.15	0.11

[a] For **13** and **14**, fit results are included for the low-energy band and the high-energy band. The spectrum of **15** was fit using three Franck-Condon bands; only the lowest and highest are reported here. The fit for the middle band of **15** (see body of paper) is included in Table 3 for sub-band 2 of compound **15**. [b] Top row of parameters was obtained from a fit with Γ fixed at 0.1 eV; parameters in parentheses were obtained with a fit with unconstrained Γ, as discussed in the text. [c] The molar extinction coefficient at the peak amplitude of the 0-0 vibronic transition in the Franck-Condon progression. [d] Vibrational frequency. [e] Energy of the peak of the 0-0 vibronic transition. [f] Huang-Rhys factor. [g] Damping width of the Gaussian components of the progression. [h] The damping width for the high-energy bands of **13** and **14** were fixed at 0.1 before performing the fit, as described in the text.

Table 3: Parameters of modified Franck-Condon fitting of Compounds **15**-**20**.

Compound	$\varepsilon_{0\text{-}0}(1)$ (l mol^{-1} cm^{-1})[a]	$\varepsilon_{0\text{-}0}(2)$ (l mol^{-1} cm^{-1})[a]	ratio[b]	$E_{0\text{-}0}(1)$ (eV)[c]	$E_{0\text{-}0}(2)$ (eV)[c]	$\Delta E_{0\text{-}0}$ ($2V_{CT}$) (eV)[d]	Γ (eV)[e]
15	62,000	20,000	3.1	2.68	2.95	0.273	0.1[f]
16	32,000	17,000	1.9	2.61	2.93	0.322	0.125
17	37,000	15,000	2.5	2.6	2.92	0.321	0.115
18	27,000	20,000	1.4	2.54	2.89	0.352	0.141
19	26,000	22,000	1.2	2.55	2.89	0.343	0.141
20	7,000	27,000	0.26	2.39	2.78	0.393	0.197

[a]In this Table, $\varepsilon_{0\text{-}0}(1)$ and $\varepsilon_{0\text{-}0}(2)$ and are the peak molar extinction coefficients of the 0-0 vibronic transitions of the two sub-bands in the broad low-energy absorption band of the donor/acceptor substituted cruciforms **15**-**20**. Sub-band 1 is the lower energy of the two Franck-Condon fits used to describe the lowest-energy band and sub-band 2 is the higher energy Franck-Condon fit. [b]The ratio $\varepsilon_{0\text{-}0}(1)$: $\varepsilon_{0\text{-}0}(2)$, showing the increasing contribution of sub-band 2 to the composition of the low-energy band of the donor/acceptor substituted cruciforms. [c]The $E_{0\text{-}0}$ values of the sub-bands. [d]$\Delta E_{0\text{-}0}$ is the gap between the 0-0 vibronic transitions in the sub-bands. [e]The damping width Γ is common to the Franck-Condon fits used in both sub-bands. The damping width for the sub-band 1 of **15** is reported as the low-energy band Γ for **15** in Table 2; the damping width of sub-band 2 of **15** is reported in the Supporting Information. [f] The independent fits of the sub-bands 1 (see Table 2) and 2 (see Supporting Information) of **15** both returned a Γ of 0.1, even though they were not constrained to the same value by the fitting procedure.

REFERENCES

(1) Albota, M.; Beljonne, D.; Bredas, J.; Ehrlich, J. E.; Fu, J.; Heikal, A. A.; Hess, S. E.; Kogej, T.; Levin, M. D.; Marder, S.; McCord-Maughon, D.; Perry, J. W.; Rockel, H.; Rumi, M.; Subramaniam, G.; Webb, W. W.; Wu, X.; Xu, C. *Science* **1998**, *281*, 1653.

(2) Reinhardt, B. A.; Brott, L. L.; Clarson, S. J.; Dillard, A. G.; Bhatt, J. C.; Kannan, R.; Yuan, L.; He, G. S.; Prasad, P. N. *Chemistry of Materials* **1998**, *10*, 1863.

(3) He, G. S.; Tan, L.; Zheng, Q.; Prasad, P. N. *Chemical Reviews* **2008**, *108*, 1245.

(4) Rumi, M.; Barlow, S.; Wang, J.; Perry, J. W.; Marder, S. *Advances in Polymer Science* **2008**, *213*, 1.

(5) Pawlicki, M.; Collins, H.; Denning, R.; Anderson, H. *Angewandte Chemie International Edition* **2009**, *48*, 3244.

(6) Denk, W.; Strickler, J.; Webb, W. *Science* **1990**, *248*, 73.

(7) Xu, C.; Webb, W. *Topics in fluorescence spectroscopy* **1997**, *5*, 471.

(8) So, P.; Dong, C.; Masters, B.; Berland, K. *Annual Review of Biomedical Engineering* **2000**, *2*, 399.

(9) Maruo, S.; Nakamura, O.; Kawata, S. *Optics Letters* **1997**, *22*, 132.

(10) Cumpston, B.; Ananthavel, S.; Barlow, S.; Dyer, D.; Ehrlich, J.; Erskine, L.; Heikal, A.; Kuebler, S.; Lee, I.; McCord-Maughon, D. *Nature* **1999**, *398*, 51.

(11) Sun, H.; Kawata, S. *Advances in Polymer Science* **2004**, *170*, 169.

(12) Lafratta, C.; Fourkas, J.; Baldacchini, T.; Farrer, R. *Angewandte Chemie International Edition* **2007**, *46*, 6238.

(13) Lee, K.; Kim, R. H.; Yang, D.; Park, S. H. *Progress in Polymer Science* **2008**, *33*, 631.

(14) Maguire, P.; Barry, L.; Krug, T.; Guo, W.; Lynch, M.; Bradley, A. L.; Donegan, J. F.; Folliot, H. *Journal of Lightwave Technology* **2006**, *24*, 2683.

(15) He, G.; Xu, G.; Prasad, P.; Reinhardt, B.; Bhatt, J.; Dillard, A. *Optics Letters* **1995**, *20*, 435.

(16) Ehrlich, J.; Wu, X.; Lee, I.; Hu, Z.; Röckel, H.; Marder, S. R.; Perry, J. W. *Optics Letters* **1997**, *22*, 1843.

(17) Charlot, M.; Izard, N.; Mongin, O.; Riehl, D.; Blanchard-Desce, M. *Chemical Physics Letters* **2006**, *417*, 297.

(18) Strehmel, B.; Sarker, A.; Detert, H. *ChemPhysChem* **2003**, *4*, 249.

(19) Rumi, M.; Ehrlich, J. E.; Heikal, A. A.; Perry, J. W.; Barlow, S.; Hu, Z.; McCord-Maughon, D.; Parker, T. C.; Rockel, H.; Thayumanavan, S.; Marder, S. R.; Beljonne, D.; Bredas, J.-L. *Journal Of The American Chemical Society* **2000**, *122*, 9500.

(20) Pond, S. J. K.; Rumi, M.; Levin, M. D.; Parker, T. C.; Beljonne, D.; Day, M. W.; Bredas, J. L.; Marder, S. R.; Perry, J. W. *Journal of Physical Chemistry A* **2002**, *106*, 11470.

(21) Ventelon, L.; Moreaux, L.; Mertz, J.; Blanchard-Desce, M. *Synthetic Metals* **2002**, *127*, 17.

(22) Kuzyk, M. G.; Dirk, C. W. *Physical Review A* **1990**, *41*, 5098.

(23) Ahn, T.; Kim, K.; Kim, D.; Noh, S.; Aratani, N.; Ikeda, C.; Osuka, A.; Kim, D. *J. Am. Chem. Soc* **2006**, *128*, 1700.

(24) Frampton, M. J., Akdas, H., Cowley, A. R., Rogers, J. E., Slagle, J. E., Fleitz, P. A., Drobizhev, M., Rebane, A., and Anderson, H. L. *Organic Letters* **2005**, *7*, 5365.

(25) Drobizhev, M.; Stepanenko, Y.; Dzenis, Y.; Karotki, A.; Rebane, A.; Taylor, P. N.; Anderson, H. L. *Journal Of The American Chemical Society* **2004**, *126*, 15352.

(26) Drobizhev, M.; Stepanenko, Y.; Dzenis, Y.; Karotki, A.; Rebane, A.; Taylor, P. N.; Anderson, H. L. *The Journal of Physical Chemistry B* **2005**, *109*, 7223.

(27) Raymond, J. E.; Bhaskar, A.; Goodson, T.; Makiuchi, N.; Ogawa, K.; Kobuke, Y. *J Am Chem Soc* **2008**, *130*, 17212.

(28) Williams-Harry, M.; Bhaskar, A.; Ramakrishna, G.; Goodson, T.; Imamura, M.; Mawatari, A.; Nakao, K.; Enozawa, H.; Nishinaga, T.; Iyoda, M. *J Am Chem Soc* **2008**, *130*, 3252.

(29) Screen, T. E. O.; Thorne, J. R. G.; Denning, R. G.; Bucknall, D. G.; Anderson, H. L. *Journal Of The American Chemical Society* **2002**, *124*, 9712.

(30) Drobizhev, M.; Stepanenko, Y.; Rebane, A.; Wilson, C. J.; Screen, T. E. O.; Anderson, H. L. *Journal Of The American Chemical Society* **2006**, *128*, 12432.

(31) Zyss, J.; Ledoux, I. *Chemical Reviews* **1994**, *94*, 77.

(32) Chung, S.; Kim, K.; Lin, T.; He, G. S.; Swiatkiewicz, J.; Prasad, P. N. *Journal of Physical Chemistry B* **1999**, *103*, 10741.

(33) Chung, S.; Lin, T.; Kim, K.; He, G. S.; Swiatkiewicz, J.; Prasad, P. N.; Baker, G. A.; Bright, F. V. *Chemistry of Materials* **2001**, *13*, 4071.

(34) Beljonne, D.; Wenseleers, W.; Zojer, E.; Shuai, Z.; Vogel, H.; Pond, S. J. K.; Perry, J. W.; Marder, S.; Bredas, J. L. *Advance Functional Materials* **2002**, *12*, 631.

(35) Cho, B. R.; Son, K. H.; Lee, S. H.; Song, Y.; Lee, Y.; Jeon, S.; Choi, J. H.; Lee, H.; Cho, M. *Journal Of The American Chemical Society* **2001**, *123*, 10039.

(36) Concilio, S.; Biaggio, I.; Günter, P.; Piotto, S.; Edelmann, M.; Raimundo, J.; Diederich, F. *Journal of The Optical Society of America B* **2003**, *20*, 1656.

(37) Derkowska, B.; Mulatier, J. C.; Fuks, I.; Sahraoui, B.; Phu, X. N.; Andraud, C. *Journal Of the Optical Society of America B* **2001**, *18*, 610.

(38) Lee, W.; Lee, H.; Kim, J.; Choi, J.; Cho, M.; Jeon, S.; Cho, B. R. *Journal Of The American Chemical Society* **2001**, *123*, 10658.

(39) McDonagh, A. M.; Humphrey, M. G.; Samoc, M.; Luther-Davies, B. *Organometallics* **1999**, *18*, 5195.

(40) Drobizhev, M.; Karotki, A.; Rebane, A.; Spangler, C. W. *Optics Letters* **2001**, *26*, 1081.

(41) Varnavski, O.; Leanov, A.; Liu, L.; Takacs, J.; Goodson, T. *Journal of Physical Chemistry B* **2000**, *104*, 179.

(42) Varnavski, O.; Yan, X.; Mongin, O.; Blanchard-Desce, M.; Goodson, T. *The Journal of Physical Chemistry C* **2007**, *111*, 149.

(43) Terenziani, F.; Katan, C.; Badaeva, E.; Tretiak, S.; Blanchard-Desce, M. *Advanced Materials* **2008**, *20*, 4641.

(44) Terenziani, F.; Le Droumaguet, C.; Katan, C.; Mongin, O.; Blanchard-Desce, M. *ChemPhysChem* **2007**, *8*, 723.

(45) Drobizhev, M.; Karotki, A.; Dzenis, Y.; Rebane, A.; Suo, Z.; Spangler, C. W. *The Journal of Physical Chemistry B* **2003**, *107*, 7540.

(46) Katan, C.; Terenziani, F.; Mongin, O.; Werts, M.; Porres, L.; Pons, T.; Mertz, J.; Tretiak, S.; Blanchard-Desce, M. *J Phys Chem A* **2005**, *109*, 3024.

(47) Yang, W.; Kim, C.; Jeong, M.; Lee, S.; Piao, M.; Jeon, S.; Cho, B. *Chem. Mater* **2004**, *16*, 2783.

(48) Katan, C.; Terenziani, F.; Le Droumaguet, C.; Mongin, O. *Proceedings of SPIE* **2005**, *5935*, 593503.

(49) Katan, C.; Tretiak, S.; Werts, M.; Bain, A.; Marsh, R.; Leonczek, N.; Nicolaou, N.; Badaeva, E.; Mongin, O.; Blanchard-Desce, M. *Journal of Physical Chemistry B-Condensed Phase* **2007**, *111*, 9468.

(50) Rumi, M.; Pond, S. J. K.; Meyer-Friedrichsen, T.; Zhang, Q.; Bishop, M.; Zhang, Y.; Barlow, S.; Marder, S. R.; Perry, J. W. *The Journal of Physical Chemistry C* **2008**, *112*, 8061.

(51) Rumi, M.; Pond, S. J. K.; Zhang, Q.; Bishop, M.; Zhang, Y.; Barlow, S.; Marder, S. R.; Perry, J. W. *Proceedings of SPIE* **2008**, *6891*, 689104/1.

(52) Slepkov, A. D.; Marsden, J. A.; Miller, J. J.; Shirtcliff, L. D.; Haley, M. M.; Kamada, K.; Tykwinski, R. R.; Hegmann, F. A. *Proceedings of SPIE* **2005**, *5934*, 593405.

(53) Slepkov, A. D., Hegmann, F. A., Tykwinski, R. R., Kamada, K., Ohta, K., Marsden, J. A., Spitler, E. L., Miller, J. E., and Haley, M. M. *Optics Letters* **2006**, *31*, 3315.

(54) Wilson, J. N.; Bunz, U. H. F. *Journal Of The American Chemical Society* **2005**, *127*, 4124.

(55) Zucchero, A. J.; Wilson, J. N.; Bunz, U. H. F. *Journal Of The American Chemical Society* **2006**, *128*, 11872.

(56) Hauck, M.; Schonhaber, J.; Zucchero, A. J.; Hardcastle, K. I.; Muller, T. J.; Bunz, U. H. *The Journal of organic chemistry* **2007**, *72*, 6714.

(57) Brombosz, S. M.; Zucchero, A. J.; Phillips, R. L.; Vazquez, D.; Wilson, A.; Bunz, U. H. *Organic Letters* **2007**, *9*, 4519.

(58) Tolosa, J.; Zucchero, A. J.; Bunz, U. H. F. *Journal Of The American Chemical Society* **2008**, *130*, 6498.

(59) Ritchie, C. D.; Sager, W. F. An Examination of Structure-Reactivity Relationships. In *Progress in Physical Organic Chemistry*; Cohen, S. G., Streitwieser, A., Jr., Taft, R. W., Eds., 1964; pp 323.

(60) Lide, D. R., ed. *CRC Handbook of Chemistry and Physics, 89th edition (Internet Version 2009)*; CRC Press/Taylor and Francis: Boca Raton, FL, 2008.

(61) Wilson, J. N.; Josowicz, M.; Wang, Y.; Bunz, U. H. F. *Chemical Communications* **2003**, 2962.

(62) Wilson, J. N.; Hardcastle, K.; Josowicz, M.; Bunz, U. H. F. *Tetrahedron* **2004**, *60*, 7157.

(63) Berlman, I. S. *Handbook of Fluorescence Spectra of Aromatic Molecules*; Academic Press: New York, 1971.

(64) Xu, C.; Webb, W. W. *Journal of the Optical Society of America B* **1996**, *13*, 481.

(65) Kennedy, S. M.; Lytle, F. E. *Analytical Chemistry* **1986**, *58*, 2643.

(66) Fisher, W. G.; Wachter, E. A.; Lytle, F. E.; Armas, M.; Seaton, C. *Applied Spectroscopy* **1998**, *52*, 536.

(67) Kasha, M.; Rawls, H. R.; El-Bayoumi, M. A. *Pure Appl. Chem* **1965**, 371.

(68) Ferguson, J. *Chemical Reviews* **1986**, *86*, 957.

(69) Herzberg, G. *Molecular Spectra and Molecular Structure*, 2 ed.; D. Van Nostrand Company, Inc.: New York, 1950; Vol. I. Spectra of Diatomic Molecules.

(70) Parson, W. W. *Modern Optical Spectroscopy*; Springer: New York, 2007.

(71) Cornil, J.; Beljonne, D.; Shuia, Z.; Hagler, T.; Campbell, I.; Bradley, D.; Brédas, J. L.; Spangler, C.; Müllen, K. *Chemical Physics Letters* **1995**, *247*, 425.